Cell Reports
Medicine

Article

Targeting low levels of MIF expression as a potential therapeutic strategy for ALS

Graphical abstract

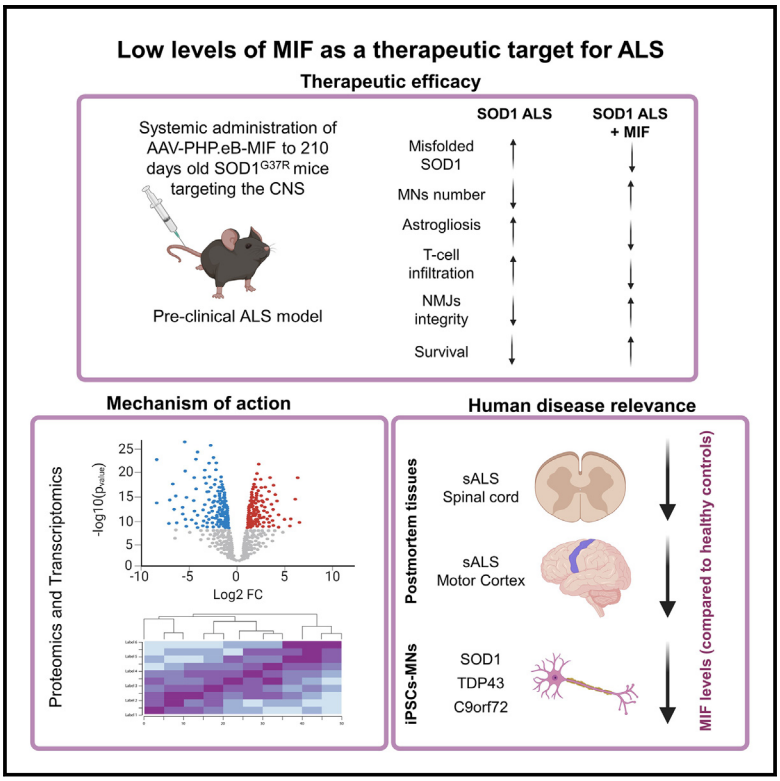

Highlights

- Systemic AAV/PhPeB MIF administration after ALS onset extends SOD1^{G37R} mice survival
- MIF positively affects pathways, including inflammation, neurogenesis, and metabolism
- Low MIF in iPSCs-MNs of SOD1, C9orf72, and TDP43 patients correspond with murine data
- Low levels of MIF are present in the motor cortex and spinal cord of sALS patients

Authors

Leenor Alfahel, Thomas Gschwendtberger, Velina Kozareva, ..., Tobias Cantz, Susanne Petri, Adrian Israelson

Correspondence

adriani@bgu.ac.il

In brief

Alfahel et al. demonstrate that systemically administered MIF following disease onset extends survival of SOD1^{G37R} mice, functioning as both a misfolded SOD1 chaperone and also affecting diverse cellular pathways. Importantly, low MIF levels are present in fALS and sALS patients, corresponding to low levels previously revealed in SOD1 mice.

Alfahel et al., 2024, Cell Reports Medicine 5, 101546
May 21, 2024
https://doi.org/10.1016/j.xcrm.2024.101546

CellPress

Cell Reports Medicine

CellPress
OPEN ACCESS

Article

Targeting low levels of MIF expression as a potential therapeutic strategy for ALS

Leenor Alfahel,[1,2,18] Thomas Gschwendtberger,[3,4,18] Velina Kozareva,[5] Laura Dumas,[6,7] Rachel Gibbs,[6,7] Alexander Kertser,[8] Kuti Baruch,[8] Shir Zaccai,[1,2] Joy Kahn,[1,2] Nadine Thau-Habermann,[3] Reto Eggenschwiler,[9,10] Jared Sterneckert,[12] Andreas Hermann,[13,14,15] Niveda Sundararaman,[16,17] Vineet Vaibhav,[16,17] Jennifer E. Van Eyk,[16,17] Victor F. Rafuse,[6,7] Ernest Fraenkel,[5] Tobias Cantz,[9,10,11] Susanne Petri,[3,4] and Adrian Israelson[1,2,19,*]

[1]Department of Physiology and Cell Biology, Faculty of Health Sciences, Ben-Gurion University of the Negev, P.O.B. 653, Beer Sheva 84105, Israel
[2]The School of Brain Sciences and Cognition, Ben-Gurion University of the Negev, P.O.B. 653, Beer Sheva 84105, Israel
[3]Department of Neurology, Hannover Medical School, 30625 Hannover, Germany
[4]Center for Systems Neuroscience, Hannover Medical School, 30625 Hannover, Germany
[5]Department of Biological Engineering, Massachusetts Institute of Technology, Cambridge, MA 02139, USA
[6]Department of Medical Neuroscience, Dalhousie University, Halifax, Nova Scotia B3H 1X5, Canada
[7]Brain Repair Centre, Life Sciences Research Institute, Halifax, Nova Scotia B3H 4R2, Canada
[8]ImmunoBrain Checkpoint Ltd., Ness Ziona 7404905, Israel
[9]Gastroenterology, Hepatology and Endocrinology Department, Hannover Medical School, 30625 Hannover, Germany
[10]Translational Hepatology and Stem Cell Biology, REBIRTH - Research Center for Translational Regenerative Medicine and Department of Gastroenterology, Hepatology and Endocrinology, Hannover Medical School, 30625 Hannover, Germany
[11]Max Planck Institute for Molecular Biomedicine, Cell and Developmental Biology, 48149 Münster, Germany
[12]Center for Regenerative Therapies Dresden, Technical University Dresden, 01307 Dresden, Germany
[13]Translational Neurodegeneration Section, "Albrecht Kossel", Department of Neurology, University Medical Center Rostock, University of Rostock, 18147 Rostock, Germany
[14]Deutsches Zentrum für Neurodegenerative Erkrankungen (DZNE) Rostock/Greifswald, 18147 Rostock, Germany
[15]Center for Transdisciplinary Neurosciences Rostock (CTNR), University Medical Center Rostock, University of Rostock, 18147 Rostock, Germany
[16]Smidt Heart Institute, Cedars-Sinai Medical Center, Los Angeles, CA 90048, USA
[17]Advanced Clinical Biosystems Research Institute, Cedars-Sinai Medical Center, Los Angeles, CA 90048, USA
[18]These authors contributed equally
[19]Lead contact
*Correspondence: adriani@bgu.ac.il
https://doi.org/10.1016/j.xcrm.2024.101546

SUMMARY

Mutations in SOD1 cause amyotrophic lateral sclerosis (ALS), a neurodegenerative disease characterized by motor neuron (MN) loss. We previously discovered that macrophage migration inhibitory factor (MIF), whose levels are extremely low in spinal MNs, inhibits mutant SOD1 misfolding and toxicity. In this study, we show that a single peripheral injection of adeno-associated virus (AAV) delivering MIF into adult SOD1^{G37R} mice significantly improves their motor function, delays disease progression, and extends survival. Moreover, MIF treatment reduces neuroinflammation and misfolded SOD1 accumulation, rescues MNs, and corrects dysregulated pathways as observed by proteomics and transcriptomics. Furthermore, we reveal low MIF levels in human induced pluripotent stem cell-derived MNs from familial ALS patients with different genetic mutations, as well as in *post mortem* tissues of sporadic ALS patients. Our findings indicate that peripheral MIF administration may provide a potential therapeutic mechanism for modulating misfolded SOD1 *in vivo* and disease outcome in ALS patients.

INTRODUCTION

Amyotrophic lateral sclerosis (ALS), the most common motor neuron disease in adults, is a fatal neurodegenerative disorder characterized by selective degeneration of both upper and lower motor neurons (MNs).[1,2] The majority of ALS cases (~90%) are sporadic, and the remaining cases are familial cases inherited in an autosomal dominant manner.[3] Nearly 20% of the familial cases are associated with missense mutations in the gene encoding cytoplasmic Cu/Zn superoxide dismutase (SOD1).[3] Although the underlying mechanism leading to the degeneration of MNs in ALS is still unknown, it has been pointed out that aberrant accumulation of misfolded SOD1 is tightly correlated with the neurotoxicity and severity of the human disease.[4–6] Transgenic mice expressing a human mutant SOD1 transgene develop MN disease[7] accompanied by accumulation of

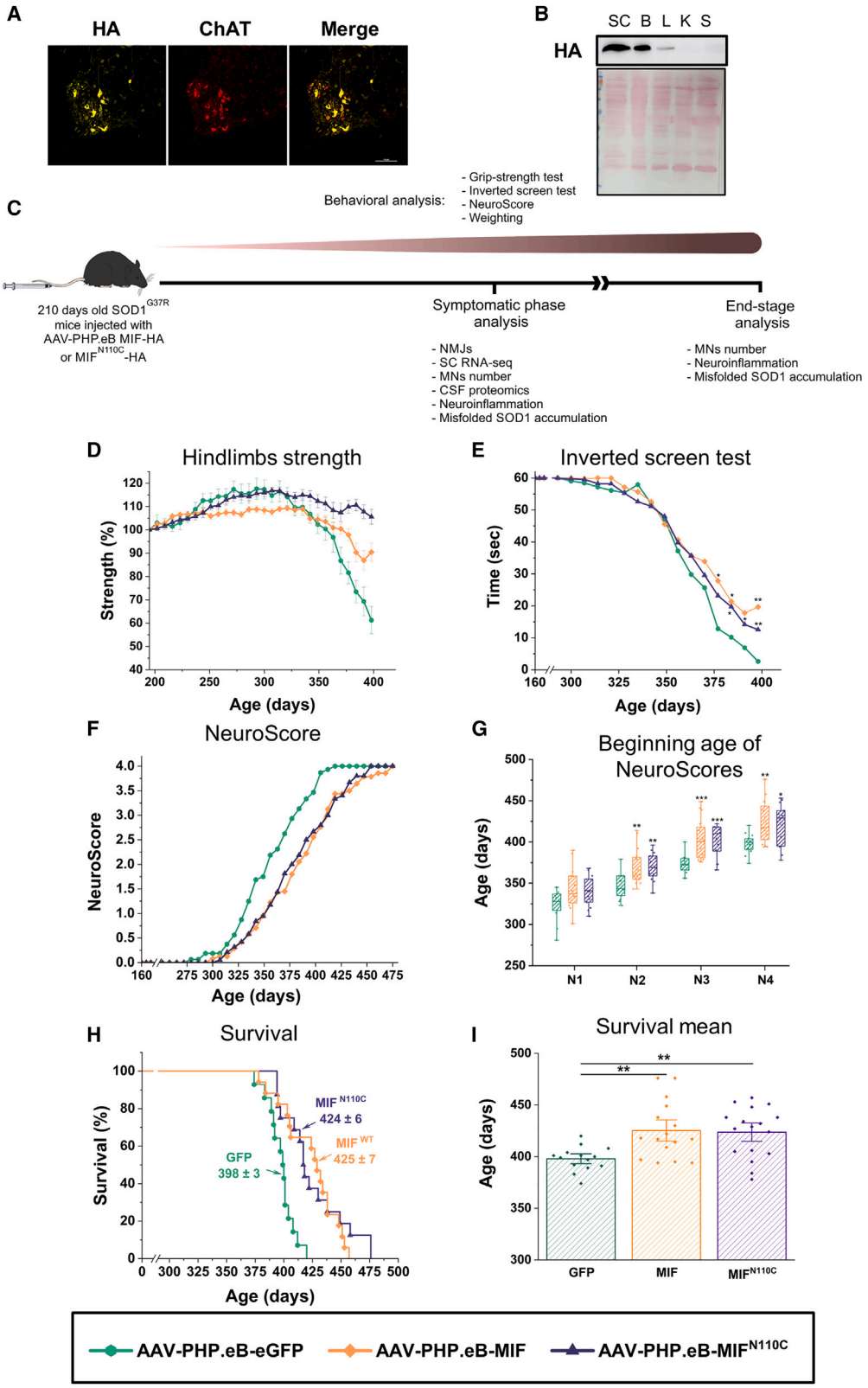

(legend on next page)

misfolded SOD1 onto the cytoplasmic surface of intracellular organelles, including mitochondria[8,9] and endoplasmic reticulum (ER).[10–12]

Previously, we have shown that macrophage migration inhibitory factor (MIF), a multi-functional protein,[13] acts as a chaperone, inhibiting the accumulation of misfolded SOD1 and its association with the spinal cord intracellular organelles and extends the survival of MNs expressing mutant SOD1.[10] Moreover, the elimination of endogenous MIF accelerates disease onset and late disease progression and shortens the survival of mutant SOD1 mice.[14] Notably, MIF protein level was shown to be extremely low in murine spinal MNs,[10,14] implicating low chaperone activity as a component of selective vulnerability of MNs to mutant SOD1 misfolding and toxicity. Finally, overexpression of MIF *in vivo* in the spinal cord of newborn transgenic mutant SOD1 mice delays disease onset and significantly extends their lifespan.[15] The delay of disease onset and progression was accompanied by a reduction of misfolded SOD1 accumulation in the spinal cord.[15]

In addition to its function as a protein-folding chaperone for misfolded SOD1,[10] MIF is a known secreted cytokine with an essential role in innate immunity.[16,17] It also functions as tautomerase and thiol-oxidoreductase,[13,18–20] and lastly as an endonuclease, under certain circumstances.[21,22] The MIF^{N110C} variant is locked in a covalent trimeric conformation formed by a disulfide bond with the Cys-80 of an adjacent subunit, in contrast to wild-type (WT) MIF, which is present as a monomer, dimer, or trimer.[23] This mutant retains partial catalytic activity and CD74 receptor binding but impaired signaling ability as a cytokine.[23] Importantly, MIF^{N110C} not only has preserved chaperone-like function but also showed total inhibition of SOD1 amyloid aggregate formation *in vitro*, suggesting that the trimeric MIF may be the preferred candidate for the MIF chaperone-like activity.[24]

In the current study, we used a more therapeutically relevant approach of peripheral adeno-associated virus (AAV) administration to overexpress MIF or MIF^{N110C} in the central nervous system (CNS) of adult mutant $SOD1^{G37R}$ mice after disease onset. We observed improved motor and neurological function, reduced neuroinflammation, reduced misfolded SOD1 accumulation, and rescue of spinal MNs accompanied with delayed progression and extended survival. Corresponding to the previously described low MIF protein in murine MNs,[10,14] we now found reduced MIF protein expression in human induced pluripotent stem cell (iPSC)-derived MNs from familial ALS patients with different genetic mutations and *post mortem* tissues from sporadic ALS patients. Finally, we show that lentiviral vector-mediated overexpression of MIF in SOD1 iPSC-derived MNs reduced the level of misfolded SOD1.

RESULTS

AAV-PHP.eB penetrates the blood-brain barrier and targets mainly the spinal MNs

To determine the efficiency of the AAV-PHP.eB vector, AAV-PHP.eB-eGFP virions at the concentration of 1.2×10^{14} vg/kg were injected to adult mice via the tail vein, as previously described.[25] Four weeks following viral administration, GFP expression was determined by immunostaining of the lumbar spinal cord and by immunoblot of protein extracts from different organs. The immunostaining images showed high expression of GFP in the spinal cord, especially in the MNs (Figure S1). The immunoblot analysis showed GFP expression mostly in the spinal cord and brain, with lower expression in the liver and no expression in the kidneys or the spleen (Figure S1), indicating a proper penetration of this vector through the blood-brain barrier (BBB), as reported previously.[26]

Subsequently, AAV-PHP.eB-MIF-HA was injected to adult mice via tail vein at the same concentration, and, 3 weeks later, the expression and localization of MIF-HA was determined. Lumbar spinal cord sections were stained using anti-HA and anti-choline acetyltransferase (ChAT) antibodies to detect MIF and MNs, respectively. HA signal was highly co-localized with the ChAT signal, indicating that the MIF expression in the spinal cord was mainly in the MNs (Figure 1A). Furthermore, the expression was tested in other organs, including non-nervous system tissues by immunoblot. MIF-HA expression was detected mainly in the spinal cord and brain, and to a lesser extent in the liver but not in the spleen or the kidneys (Figure 1B).

Overexpression of MIF or MIF^{N110C} in the spinal cord of mutant $SOD1^{G37R}$ mice after disease onset improves their motor function and neurological symptoms and extends their survival

Transgenic mutant $SOD1^{G37R}$ mice were injected at 210 days with AAV-PHP.eB-GFP (GFP), MIF^{WT}-HA (MIF), or MIF^{N110C}-HA (MIF^{N110C}) via tail-vein injection. These mice were monitored by weighing, inverted screen test, grip strength, and NeuroScore

Figure 1. Peripheral delivery of AAV-PHP.eB-MIF or AAV-PHP.eB-MIF^{N110C} to mutant $SOD1^{G37R}$ mice after disease onset improves their motor function and neurological symptoms and extends their survival

(A) Immunofluorescence staining of the lumbar spinal cord of AAV-PHP.eB-MIF-HA-treated mice 3 weeks following tail-vein injection was detected by anti-HA antibody (yellow) co-stained with anti-ChAT antibody (red). Scale bar: 100 μM.

(B) Immunoblot detection of AAV-PHP.eB-MIF-HA using anti-HA antibody in the spinal cord (SC), brain (B), liver (L), kidney (K), and spleen (S) 3 weeks following tail-vein injection.

(C) Schematic representation of the experimental design using smart Servier Medical Art, licensed under a Creative Commons Attribution 3.0 Unported License. AAV PHP.eB-MIF-HA, AAV PHP.eB-MIF^{N110C}-HA, or AAV PHP.eB-eGFP were delivered via tail-vein injection after disease onset.

(D) Hindlimb strength (%) measured by a grip-strength meter.

(E) Hanging time (seconds) in inverted screen test.

(F and G) NeuroScore measurement (F) and the age at the beginning of each NeuroScore (G).

(H and I) Survival (%) (H) and mean survival ± SEM (I) of $SOD1^{G37R}$ mice injected with AAV-PHP.eB-eGFP, green, $n = 16$ (D–G), $n = 14$ (H and I); $SOD1^{G37R}$ mice injected with AAV PHP.eB-MIF, orange, $n = 15$ (D–G), $n = 16$ (H and I); $SOD1^{G37R}$ mice injected with AAV-PHP.eB-MIF^{N110C}, purple, $n = 14$ (D–G), $n = 17$ (H and I). Statistics were performed using one-way ANOVA followed by Tukey's multiple comparison test. $^{***}p < 10^{-3}$, $^{**}p < 0.01$, $^{*}p < 0.05$. See also Figures S1, S2, S3.

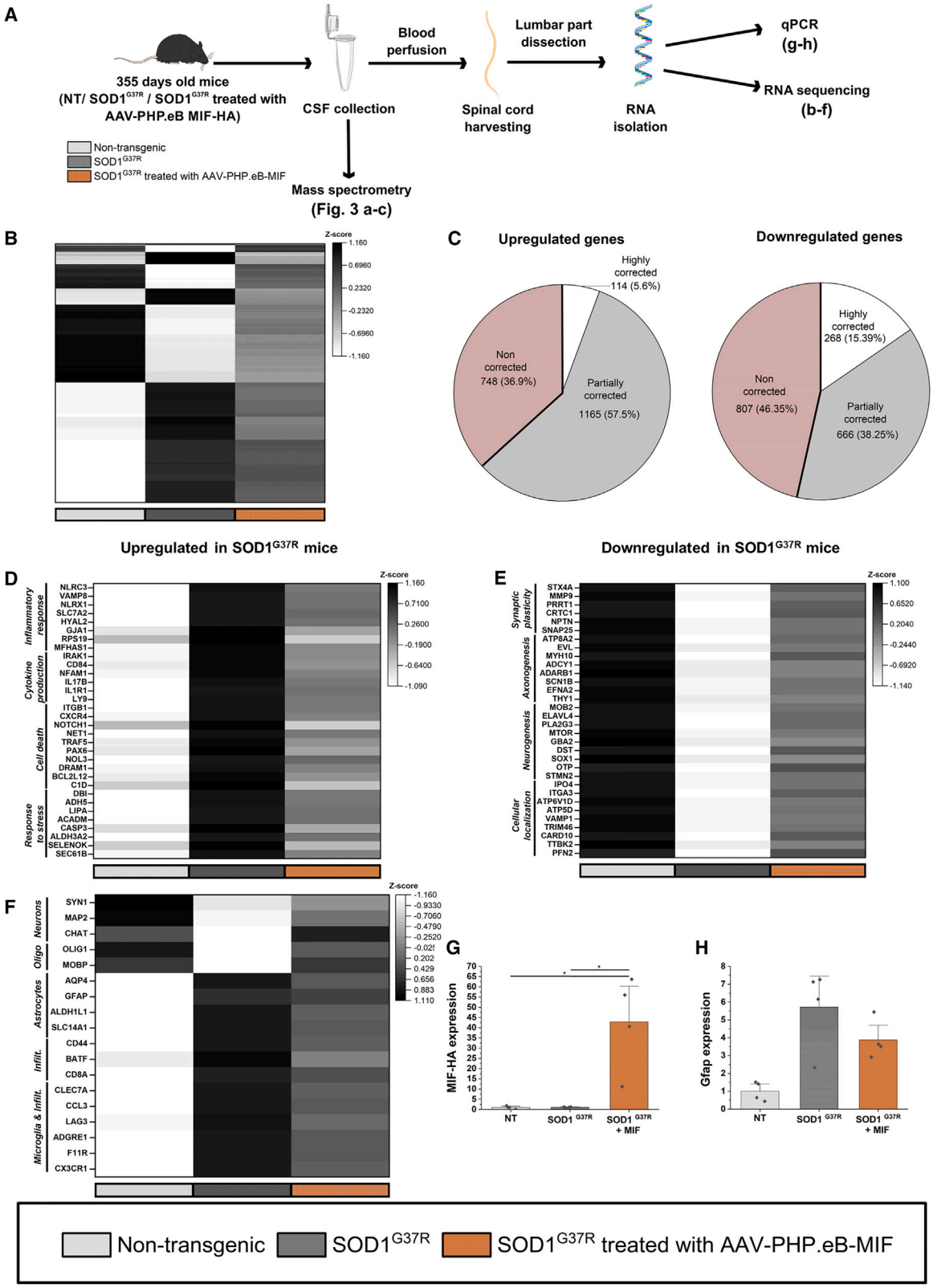

(legend on next page)

from the age of 160 days until their end stage (Figure 1C). Mutant SOD1^{G37R} mice injected with MIF or MIF^{N110C} maintained their hindlimb (Figure 1D) and total limb strength (Figure S2) longer than the GFP-injected group, who started to lose their hindlimb strength around the age of 330 days. Moreover, the inverted screen test shows that the MIF or MIF^{N110C}-treated mice were able to suspend longer than the GFP-injected mice from the age of 350 days (Figure 1E). NeuroScore of the mice shows a slower disease progression in the MIF or MIF^{N110C}-treated mice; they reached a NeuroScore of 2, 3, or end stage later than the GFP-injected group (Figures 1F and 1G). Furthermore, there was a trend for neuromuscular junctions (NMJs) of MIF-treated SOD1^{G37R} mice to be better preserved (innervated) in the plantaris (39.07%) and the soleus muscle (63.11%) compared to SOD1^{G37R} non-injected mice (14.34% and 45.92%, respectively) (Figure S3).

A simple and objective measure of disease onset and progression was applied by monitoring the initiation and progression of weight loss, respectively, mainly as a reflection of denervation-induced muscle atrophy. While progression from onset through early disease phase was only modestly affected by MIF treatment, total disease progression was significantly slowed down (Figure S2). Finally, mutant SOD1^{G37R} mice treated with either MIF or MIF^{N110C} showed an extended survival of about 4 weeks compared to the GFP-injected group (Figures 1H and 1I).

Overexpression of MIF in the nervous system partially corrects the expression of several genes that were altered in symptomatic mutant SOD1^{G37R} mice

RNA for RNA sequencing analysis was isolated from the lumbar area of the spinal cord of non-transgenic (NT), SOD1^{G37R}, and SOD1^{G37R} mice treated with MIF at the age of 355 days (Figure 2A). Since there was no additional benefit for MIF^{N110C} over the MIF^{WT}-injected group, only the MIF^{WT}-treated group was analyzed. A total of 3,856 genes were significantly changed between the NT and SOD1^{G37R} mice (Figure S4), of which 2,115 were upregulated and 1,741 were downregulated (Figures 2B and 2C). MIF treatment was able to correct, at least partially, 63.1% of the upregulated and 53.6% of the downregulated genes in SOD1^{G37R} mice, as indicated by gene hierarchical clustering (Figure 2C). Gene Ontology (GO) enrichment analysis using ShinyGO[27] shows that MIF overexpression corrected upregulated genes, including genes related to inflammatory response, cytokine production, cell death, phagocytosis, gliogenesis, response to oxidative stress, and lipid oxidation, while MIF treatment corrected downregulated genes, including genes related to nervous system development, axonogenesis, neurogenesis, synaptic signaling, neurotransmitter transport, learning, and memory (Figures 2D, 2E, and Table S1). Furthermore, although we did a bulk RNA sequencing, we examined the expression of cell-specific genes according to the mouse brain single-cell RNA sequencing by Han et al..[28] A group of genes related to astrocytes, microglia, or infiltrated immune system cells was upregulated in SOD1^{G37R} mice compared to NT mice and this was partially corrected (the expression tended toward the NT group but was not fully corrected) following MIF treatment. On the other hand, a group of genes reported to be related to oligodendrocytes or neurons (including MNs) was found to be downregulated in SOD1^{G37R} mice compared to NT mice and was partially corrected with MIF treatment (Figure 2F). Interestingly, although the MIF signaling pathway activates CXCR4 and CD44,[29–32] the RNA levels of CXCR4 and CD44 were higher in the untreated SOD1^{G37R} mice compared to MIF-treated SOD1^{G37R} mice. In order to verify the efficacy of our treatment, we tested human MIF levels in the three different groups using qPCR. Our results indicate a significant upregulation of human MIF in the treated mice spinal cords (Figure 2G). Moreover, taking into consideration that Glial fibrillary acidic protein (GFAP) is a well-known marker for activated astrocytes, we performed qPCR on the extracted RNA, showing the upregulation of GFAP in SOD1^{G37R} mice compared to NT mice, and the partial correction in the MIF-treated group (Figure 2H).

Upregulation of MIF in the nervous system partially corrects the expression of altered proteins in the CSF of symptomatic mutant SOD1^{G37R} mice

Due to its ability to spread inflammatory proteins throughout the nervous system and its essential role in maintaining CNS homeostasis,[33] the cerebrospinal fluid (CSF) has been linked to ALS. Thus, we investigated whether MIF treatment was able to alter the protein composition of the CSF. We identified 497 proteins in the CSF, out of which 37 proteins were significantly upregulated and 34 proteins were significantly downregulated in the CSF of symptomatic SOD1^{G37R} mice compared to NT mice (Figure S5). The upregulated proteins were found to be related to GO pathways such as inflammatory response, immune response,

Figure 2. Overexpression of MIF in the nervous system partially corrects the expression of several genes that were altered in symptomatic mutant SOD1^{G37R} mice

(A) Experimental design for CSF isolation for proteomics and RNA isolation for RNA sequencing analysis from 355-day-old mice using smart Servier Medical Art, licensed under a Creative Commons Attribution 3.0 Unported License.

(B) Heatmap of all the genes that were significantly altered in SOD1^{G37R} (gray, $n = 10$) compared to non-transgenic (NT) mice (white, $n = 10$) and were at least partially corrected in the MIF-treated mice (orange, $n = 4$).

(C) Pie charts of all the upregulated or downregulated genes in the spinal cord of the mutant SOD1^{G37R} compared to NT mice, representing the portion of highly corrected, partially corrected, and non-corrected genes in AAV-PHP.eB-MIF-treated compared to -untreated SOD1^{G37R} mice.

(D and E) Heatmaps of the expression of representative genes that were significantly upregulated (D) or downregulated (E) in SOD1^{G37R} compared to NT mice, ordered according to their Gene Ontology (GO) pathways.

(F) Heatmaps of the expression of representative genes related to microglia, astrocytes, neurons, oligodendrocytes (Oligo), or infiltrated cells (Infilt.).

(G and H) qPCRs for relative expression of MIF-HA (G) or GFAP (H) in the NT ($n = 4$), SOD1^{G37R} ($n = 4$), or SOD1^{G37R} treated with MIF ($n = 4$), normalized to GAPDH expression.

Graphs represent mean ± SEM. The heatmaps were generated using the Z score of the gene expression. Statistics were performed using one-way ANOVA followed by Tukey's multiple comparison test. $p < 0.05$. See also Figure S4 and Table S1.

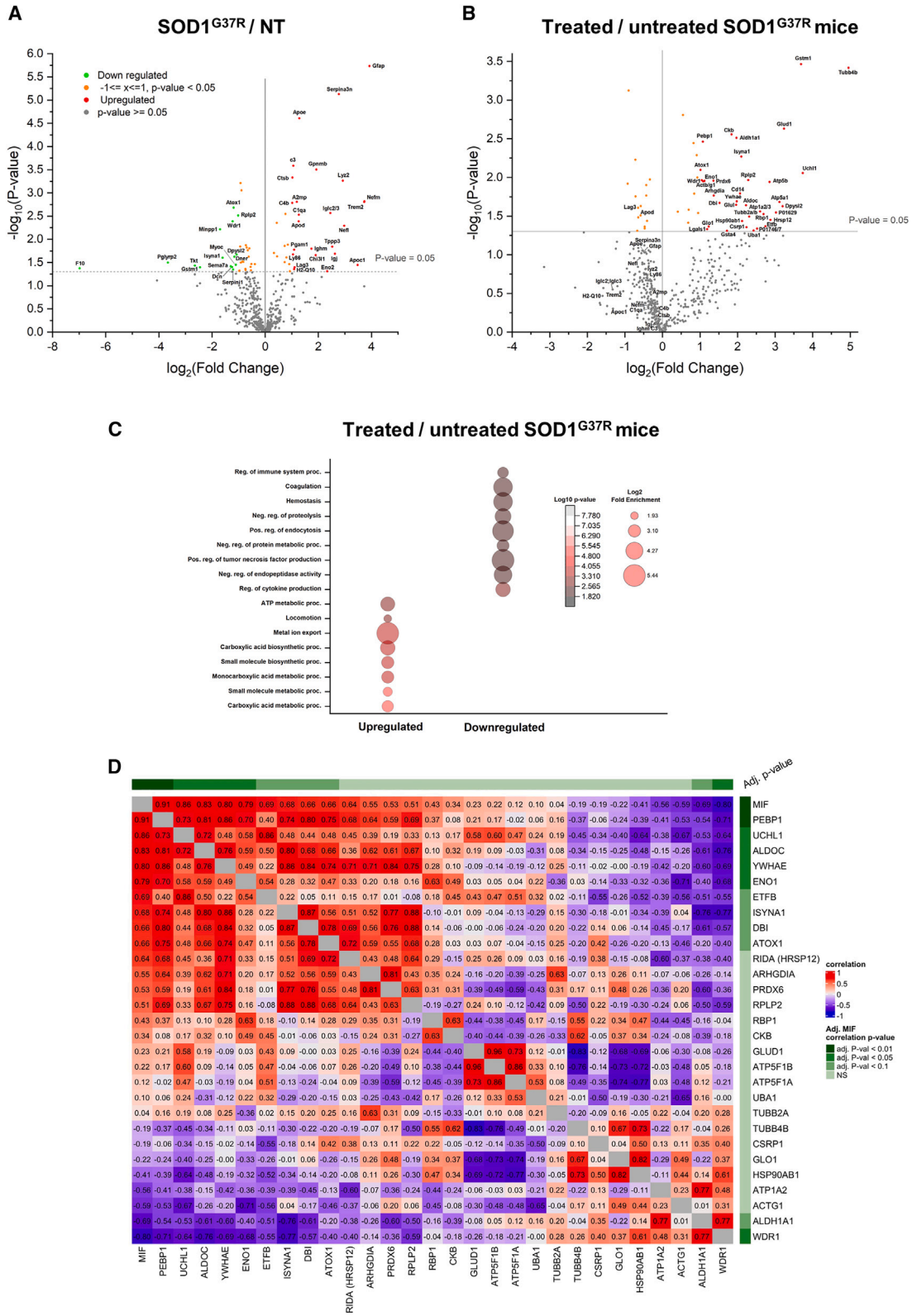

(legend on next page)

synapse pruning, and cell junction disassembly, while the downregulated proteins were found to be related to pathways such as synaptic signaling, neurogenesis, and regulation of nervous system development (Figure S5). Part of the upregulated proteins in the SOD1^{G37R} mice are well-known inflammatory proteins such as GFAP and Trem2, and the neurofilaments Nefl and Neflm (light and medium), which are markers for axonal damage and cell death (Figures 3A, and S5). As for the downregulated proteins, some of them are metabolic proteins such as Minnp1, Isyna1, and Tkt; some are related to CNS development, such as Dner, Dpysl2, and Sema7A; as well as antioxidants such as Atox1. Importantly, MIF overexpression resulted in upregulation of Isyna1, Atox1, Rplp2, Dpysl2, and Gstm1, which were downregulated in the SOD1^{G37R} mice and a clear trend of downregulation of GFAP, Trem2, and the neurofilaments that were upregulated in SOD1^{G37R} mice (Figures 3B, and S5). Furthermore, the overexpression of MIF resulted in the upregulation of the neurogenesis pathway, which was downregulated in the SOD1^{G37R} mice and the upregulation of metal ion export pathway and different metabolic pathways that were found to be defective in ALS,[34,35] along with downregulation of inflammatory pathways as regulation of immune system processes and cytokine production that are upregulated in ALS (Figure 3C). Of the cell-specific genes (Figure 2F), GFAP and LAG3 were found in the CSF proteomics analysis too, and were both found to be partially corrected, with a reduction of 27% and 36% following MIF treatment, with $p = 0.092$ and 0.024, respectively.

To examine whether similar effects are seen in human data, we analyzed the Answer ALS dataset (https://www.answerals.org) (Figure 3D), which was established with the aim to generate 1,000 iPSC lines differentiated to MNs from patients with all forms of ALS who have deep clinical data along with whole-genome sequencing and multi-omics.[36] Strikingly, several of the upregulated proteins in the MIF-treated SOD1^{G37R} mice are also significantly positively correlated with MIF in iPSC MNs derived from SOD1 cases in the Answer ALS dataset. Indeed, nine of the 28 most upregulated proteins in the MIF-treated mice are significantly positively correlated with MIF expression (Pearson correlation, false discovery rate [FDR] <0.1), with additional proteins showing weaker positive associations with MIF. A small number of proteins, including cytoskeletal organization proteins, show weak or negative correlation with MIF expression in the iPSC MNs (Figure 3D). Moreover, similar protein correlation patterns are observed across all ALS cases in the Answer ALS dataset (15 of 28 upregulated proteins are positively associated with MIF, Pearson correlation FDR <0.05), suggesting that MIF expression could have similar molecular effects in MNs more broadly in sporadic ALS (Figure S6). In addition, among all proteins quantified in the Answer ALS iPSC-MNs dataset, those highly correlated with MIF expression were significantly enriched for the set of MIF-treated upregulated proteins in Figure 3B, for both SOD1 cases (mHG test $p = 0.00084$) and across sporadic ALS cases (mHG test $p = 0.00019$).

Overexpression of MIF in the nervous system after disease onset reduces astrogliosis and T cell infiltration into the spinal cord of mutant SOD1^{G37R} mice

Non-cell-autonomous mechanisms play an important role in the pathology of neurodegenerative diseases in general, and in ALS specifically,[37] where overactivation of astrocytes and microglia together with infiltration of T cells into the spinal cord were shown to be crucial for driving disease progression.[38–40] Immunostaining (Figures 4A and 4G) and immunoblot analysis (Figure 4D) were performed to determine the levels of activated astrocytes (detected by GFAP antibody) and microglia (detected by Iba-1 antibody) in the lumbar spinal cord of mutant SOD1^{G37R} mice. Symptomatic mutant SOD1^{G37R} mice treated with MIF or MIF^{N110C} showed a reduction in activated astrocytes as shown by immunostaining (Figures 4A and 4B) and immunoblot analysis (Figures 4D and 4E) but no significant change in microglia (Figures 4A–4C, and 4F) in the lumbar spinal cord compared to non-injected mice. Immunostaining of the lumbar spinal cords of SOD1^{G37R} mice at the end stage of the disease confirmed these findings, showing a similar significant reduction in activated astrocytes but no significant reduction in microglia in MIF or MIF^{N110C}-treated SOD1^{G37R} mice (Figures 4G–4I). Moreover, immunostaining was performed to determine the infiltration of T cells (detected by CD3 and CD4 antibodies) in the lumbar spinal cord of mutant SOD1^{G37R} mice. Symptomatic and end-stage mutant SOD1^{G37R} mice treated with MIF after disease onset showed reduced infiltration of T cells into the lumbar spinal cord (Figure S7).

MIF or MIF^{N110C} upregulation in the nervous system of mutant SOD1^{G37R} mice after disease onset reduces misfolded SOD1 accumulation and rescues spinal MNs

Similar to ALS patients, MN degeneration is also observed in the spinal cord of mutant SOD1 mouse models. To determine the number of MNs and the levels of misfolded SOD1 in the lumbar spinal cord of SOD1^{G37R} mice, we used an anti-ChAT antibody and B8H10 antibody, respectively. Immunostaining of the lumbar spinal cord at the disease end stage showed increased levels of ChAT-positive MNs (Figures 5A–5C), accompanied by reduction of misfolded SOD1 (Figures 5A and 5B) in MIF or MIF^{N110C}-treated mice compared to GFP-injected mice, indicating reduced misfolded SOD1 accumulation and MNs rescue as a

Figure 3. Upregulation of MIF in the nervous system partially corrects the expression of altered proteins in the CSF of symptomatic mutant SOD1^{G37R} mice

(A and B) Volcano plots of proteomics data. The –log (*p* value) plotted against the log2 of the fold change of proteins in the CSF of SOD1^{G37R} ($n = 3$) compared to NT mice ($n = 4$) (A) or proteins in the CSF of AAV-PHP.eB-MIF-treated ($n = 4$) compared to -untreated SOD1^{G37R} mice ($n = 4$) (B).

(C) Colored bubble plot representing the upregulated and downregulated GO pathways in the AAV-PHP.eB-MIF-treated compared to -untreated SOD1^{G37R} mice. The color of the bubble represents the log10 of the *p* value of the pathway, and the bubble size represents the fold enrichment of the pathways.

(D) Heatmap showing correlation across protein expression in iPSC MNs derived from SOD1 patients in the Answer ALS dataset ($n = 10$) for proteins that were significantly upregulated following MIF treatment in (B). Columns and rows sorted by expression correlation with MIF. Green annotation bar (top) indicates significance (FDR adjusted) of Pearson correlation of protein in column with MIF expression. See also Figures S5, and S6.

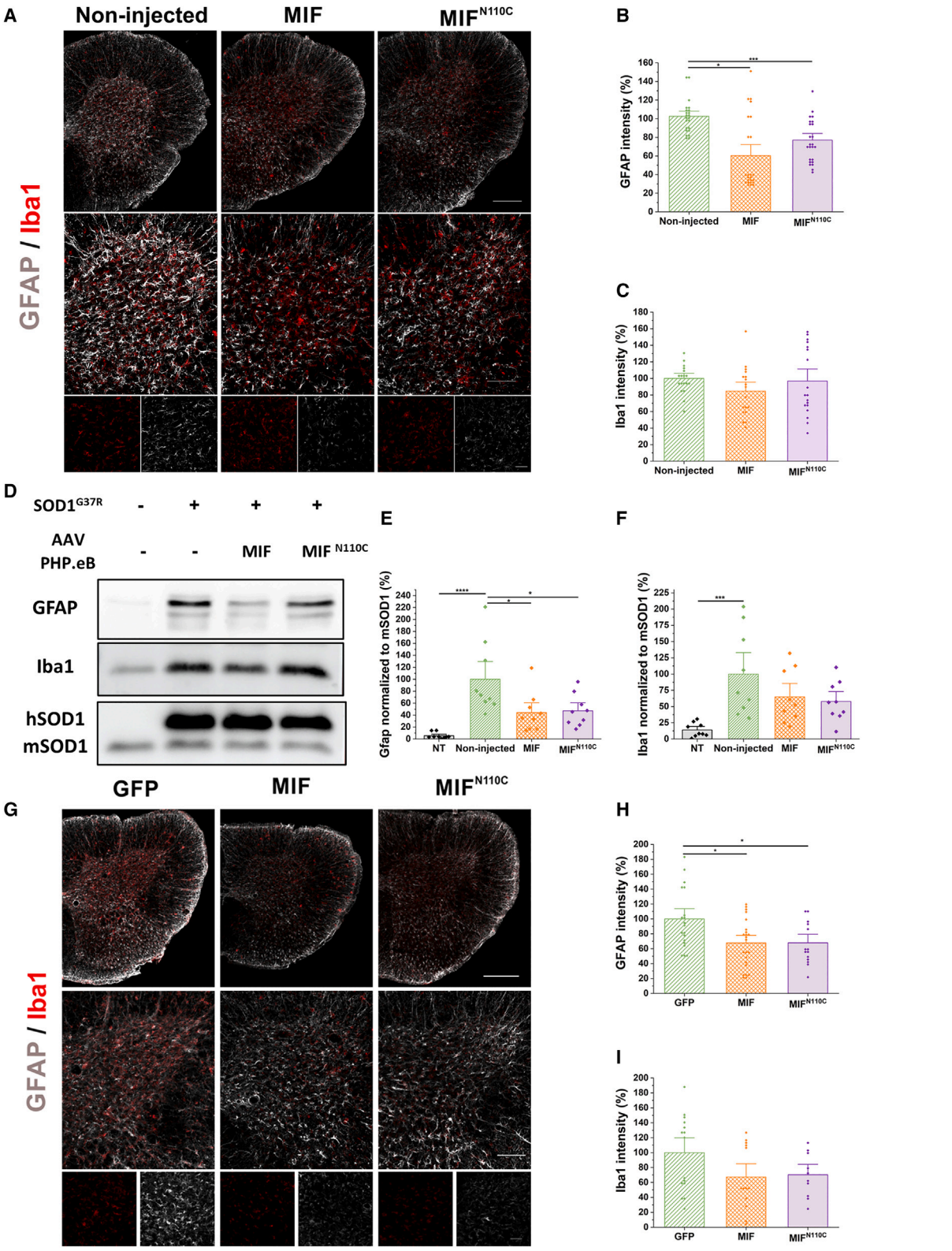

(legend on next page)

result of MIF treatment after disease onset. Furthermore, ChAT and B8H10 staining of the lumbar spinal cord of symptomatic SOD1^{G37R} mice likewise showed rescue of spinal MNs and reduction of misfolded SOD1 accumulation in MIF or MIF^{N110C}-treated mice (Figures 5F–5H). Moreover, misfolded SOD1 levels at disease end stage were also determined by immunoprecipitation (IP) using B8H10 antibody (Figure 5D). MIF or MIF^{N110C}-treated mice showed a reduction in misfolded SOD1 accumulation compared to GFP-injected mice (Figures 5D and 5E).

Decreased expression of MIF in MNs from ALS-patient-derived iPSCs carrying different mutations and in human *post mortem* tissue

To investigate the expression level of MIF in ALS and healthy MNs, we differentiated MNs starting from the expandable population of human induced pluripotent patient and control stem cell line (iPSCs)-derived small molecular neural progenitor cells (smNPCs). Three cell lines of healthy controls, two cell lines of ALS-SOD1 patients (one carrying a homogeneous D90A mutation and the other heterozygous R115G mutation), three cell lines with mutations in the C9orf72 gene (>50 repeats $(G4C2)_x$, ~730 repeats $(G4C2)_x$ and with ~1000 repeats $(G4C2)_x$), two cell lines of patients carrying point mutations in the TARDBP gene, which encodes the protein TDP43 (transactive response DNA binding protein 43 kDa) (G294V and S393L), and one cell line of a patient with an R521C mutation in FUS gene were used.

Detailed characterization regarding expression of neuronal and motor neuronal markers as well as MIF using immunocytochemistry was performed (Figure 6A). The results show a similar percentage of MNs across patient cell lines (Figures 6B and 6C), while MIF protein levels were found to be significantly lower in the SOD1, C9orf72, and TDP-43 lines (Figure 6D). In addition, the accumulation of misfolded SOD1 (recognized by the B8H10 antibody) was analyzed in both SOD1 and healthy control cell lines, showing a significant accumulation of misfolded SOD1 in the SOD1 lines (Figure 6E). Of note, although there were significant differences in MIF protein levels, there were no differences in MIF mRNA expression in the iPSC-derived MNs as detected by RT-qPCR (Figure 6F).

Furthermore, protein expression of MIF was analyzed by western blot analysis in human *post mortem* tissue (motor cortex and spinal cord specimens) of patients with a diagnosis of definitive or probable ALS according to the El Escorial criteria and compared to *post mortem* tissue of patients with no evidence of neurological disease. We observed a significant reduction in MIF protein expression (normalized to α-tubulin) in spinal cord and motor cortex tissue of sporadic ALS (sALS) patients compared to healthy controls (Figures 6G, H, and S8). Similarly, MIF protein levels were found to be lower in the lumbar spinal cord of SOD1^{G93A} mice at different stages of the disease as indicated by immunoblot analysis (Figure S8).

Lentiviral transduction of mutant SOD1 iPSC-derived MNs with MIF reduces SOD1 misfolding

After confirmation of reduced MIF protein expression in human ALS iPSC-derived MNs and *post mortem* CNS tissue, we attempted to reproduce the beneficial effect of MIF overexpression in a human *in vitro* model. SOD1-smNPCs and healthy control cells were transduced with MIF-overexpressing lentiviral vectors and then differentiated into MNs. Quantitative analysis of MIF and misfolded SOD1 protein expression in human iPSC-derived mutant SOD1 MNs showed a significant increase in MIF expression and significant reduction of misfolded SOD1 after MIF transduction in relation to TUJ-positive (neuron-specific class III beta-tubulin) cells and in relation to Islet-1-positive cells (Figures 7A–7D).

DISCUSSION

We have previously shown that injection of AAV2/9-MIF intrathecally into newborn mutant SOD1 transgenic mice delays their disease onset and significantly extends their lifespan.[15] However, ALS is a late-onset disease, with disease only becoming apparent once symptoms appear, thus we aimed in this study to present a more therapeutically relevant approach, where we upregulate MIF in ALS mice only after disease onset. Furthermore, potential side effects of lumbar puncture and adverse events described in relation to intrathecal delivery, e.g., in recent ALS clinical trials,[41] made us choose a less invasive approach for viral administration, namely peripheral tail-vein injection. To this end, we utilized the AAV-PHP.eB system, which was shown to efficiently penetrate the BBB.[26] Furthermore, this system of gene expression does not require genome integration and virions are replication deficient, reducing oncogenic concerns, and evidence of an AAV-mediated transgene expression was found in the human brain 10 years after administration,[42] suggesting that the virus may be long lasting in terminally differentiated cells such as MNs, potentially allowing a single dose.

Figure 4. Overexpression of MIF or MIF^{N110C} in the nervous system of mutant SOD1^{G37R} mice after disease onset reduces astrogliosis in the spinal cord

(A and G) Immunofluorescence staining of the ventral region of the lumbar spinal cord at the symptomatic stage (A) or end-stage (G) of the disease stained for activated astrocytes (GFAP, gray) and microglia (Iba-1, red).

(B and H) Quantification of the intensity of GFAP in the ventral horn of the lumbar spinal cord at the symptomatic (n = 3) (B) or end-stage (n = 4) (H) of the disease, normalized to the non-injected (n = 3) or GFP-injected group (n = 4).

(C and I) Quantification of the intensity of Iba-1 in the ventral horn of the lumbar spinal cord at the symptomatic (n = 3) (B) or end-stage (n = 4) (H) of the disease, normalized to the non-injected (n = 3) or GFP-injected group (n = 4).

(D) Immunoblot analysis of activated astrocytes (GFAP) and microglia (Iba-1) in the lumbar spinal cord of NT, non-injected, MIF-treated, or MIF^{N110C}-treated SOD1^{G37R} mice.

(E and F) Quantification of GFAP (E) and Iba-1 (F) in the spinal cord normalized to non-injected group (n = 4). Endogenous SOD1 (mSOD1) was used as loading control.

Graphs represent mean ± SEM.Statistics were performed using one-way ANOVA followed by Tukey's multiple comparison test or using Kruskal-Wallis one-way ANOVA followed by Dunn's multiple comparison test. Scale bars, 200, 100, and 50 μm. ****$p < 10^{-4}$, ***$p < 10^{-3}$, *$p < 0.05$. See also Figure S7.

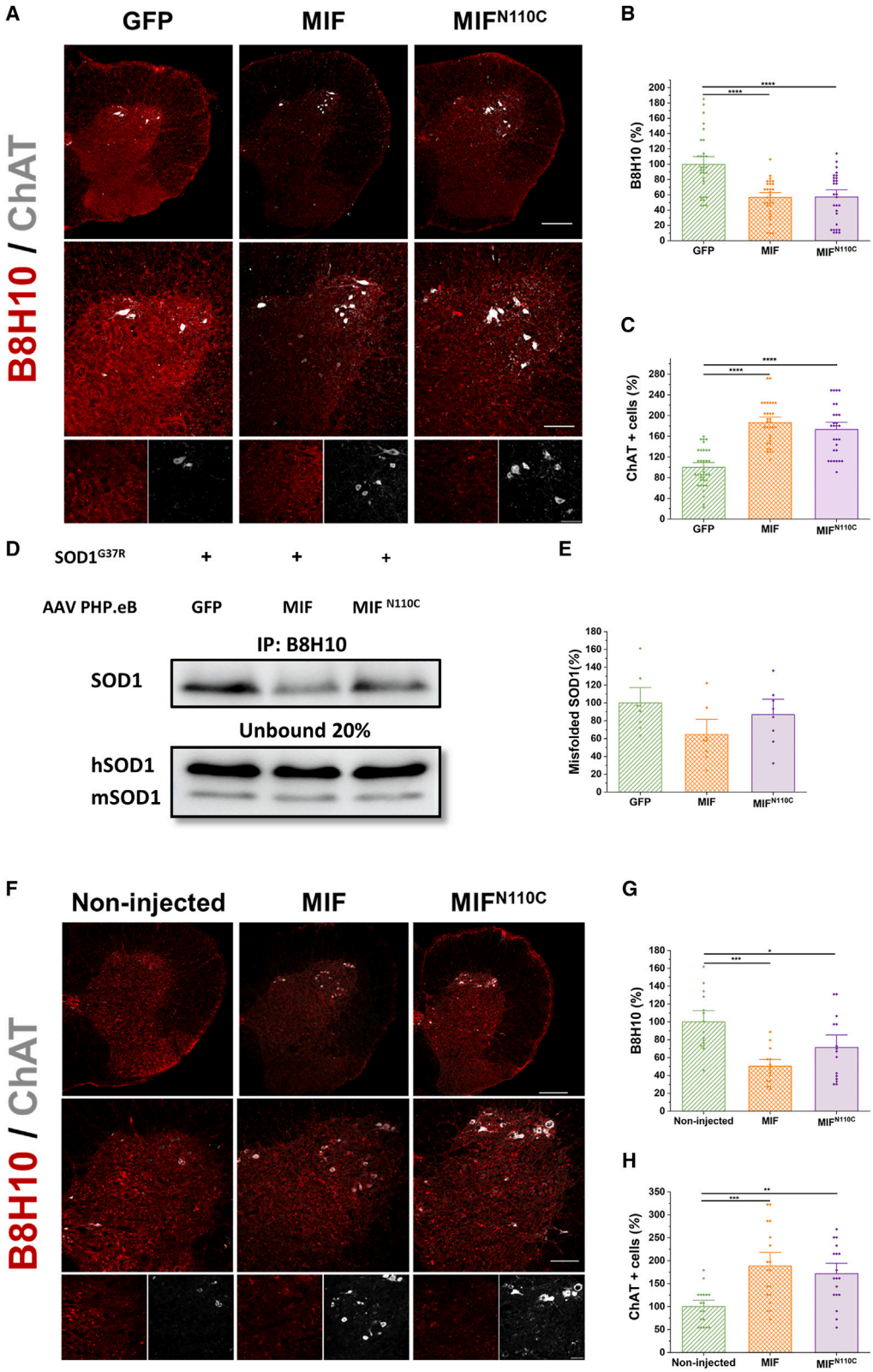

(legend on next page)

However, there may be systemic side effects, which might require further study in more advanced models to ensure its safety.

Our results indicate that injection of AAV-PHP.eB-MIF or AAV-PHP.eB-MIF^{N110C} to mutant SOD1^{G37R} mice after the disease onset indeed was able to penetrate the BBB with high expression in spinal cord MNs and brain and succeeded in improving their motor and neurological function, reduced neuroinflammation and misfolded SOD1 accumulation, rescued MNs, and, importantly, extended their survival significantly.

Contrary to our expectation, injection of the covalently locked trimeric conformation mutant MIF^{N110C} did not show any advantage over the injected WT form of MIF. These results indicate that, although the MIF^{N110C} showed better inhibition of misfolded SOD1 aggregation *in vitro*,[24] MIF (both WT and N110C) function is not mutually exclusive to inhibition of SOD1 aggregation but may be affecting several different pathways, including neurogenesis, since MIF was previously associated with cell proliferation, neurite outgrowth, and promoting cell survival and proliferation of neural stem cells.[43–46] In addition, it may affect inflammatory pathways that do not include MIF's signaling ability as a cytokine, since MIF^{N110C} has an impaired cytokine signaling activity.[23]Furthermore, the observed beneficial effect of MIF also does not involve the monomer to oligomer transition of MIF, and it is also not exclusive to the trimeric conformation since the WT form of MIF, which can exist as monomers, dimers, and trimers,[47] showed the same effect as the locked trimer MIF^{N110C} mutant.[23] Nevertheless, it is possible that the observed effect is driven by a feedback mechanism. In this scenario, the inhibition of SOD1 aggregation may likely lead to a reduction in neuroinflammation. Simultaneously, the impact of MIF on inflammatory pathways may indirectly inhibit SOD1 aggregation and its associated toxicity.

As a means to unveil these different pathways, we examined differences in RNA and protein expression of MIF-treated mice compared to their untreated counterparts. Via spinal cord RNA sequencing analysis, we revealed upregulation of the inflammatory response, cytokine production, response to stress, and cell death in mutant SOD1^{G37R} mice, with downregulation of RNA related to nervous system development, axonogenesis, and neuronal differentiation pathways when compared to NT mice. MIF-treated mice showed at least a partial correction toward an NT mice RNA profile in the mentioned pathways, among others. Notably, although MIF was mainly overexpressed in the MNs, the treatment affected the expression of genes that were previously reported to be related to other cell types in single-cell RNA sequencing,[28] including astrocytes and microglia, which play an essential role in driving disease progression in the late phase.[38,39] Moreover, although the MIF signaling pathway is known to activate CXCR4 and CD44,[29–32] we observed higher RNA levels of CXCR4 and CD44 in the untreated SOD1^{G37R} mice compared to MIF-treated SOD1^{G37R} mice. These higher RNA levels of CXCR4 and CD44 are probably a result of the increased neuroinflammatory state in the spinal cord of untreated mice, including more activated astrocytes and infiltrated T cells,[40,48–52] as also indicated by other upregulated genes in the untreated mice, such as BATF CD8a, GFAP, and AQP4. It was previously shown that, in ALS, CXCR4 leads to the downstream release of tumor necrosis factor alpha (TNFα), which binds to its receptor on the glial membrane and in turn triggers glutamate release that eventually leads to neuronal death, and that inhibition of CXCR4 by AMD3100 was effective in SOD1^{G93A} mice when administered at early stages.[53,54] On a protein level, analysis of the CSF profile of SOD1^{G37R} mice revealed upregulation in inflammatory proteins and neurofilaments, a known hallmark for neurodegeneration, and downregulation of metabolic and CNS development proteins. Supporting these findings are several studies suggesting defects in metabolic pathways as a mechanism for neurodegeneration in general, and ALS in particular, due to the high energy demand in the nervous system.[55,56] MIF treatment was able to upregulate part of the neurogenesis and metabolic pathway-related proteins. Moreover, the metal ion export pathway was found to be upregulated with a high fold enrichment as was observed by the upregulation of Atox1, Ywhae, Atp1a2, and Atp1a3 (part of the α subunit of Na+/K+-ATPase), out of 47 proteins involved in the pathway. The upregulation of these proteins specifically might be explained by the involvement of Atox1 in the mitogen-activated protein kinase (MAPK) pathway[57] and the involvement of Ywhae and Na+/K+-ATPase α subunit in MAPK and PI3K signaling pathways,[58–62] which are activated by MIF.[63–65] Notably, many metabolic-related upregulated proteins in the mouse CSF were highly correlated with MIF protein expression in the Answer ALS iPSCs-derived MNs database, both in the whole dataset and specifically in the SOD1 cases, suggesting MIF involvement in these metabolic pathways in cells derived from ALS patients as well, and implying its beneficial potential.

Revealing the important role of MIF in slowing ALS disease progression in a murine model resulted in a need to understand the role of MIF in human disease based on the limitation

Figure 5. MIF or MIF^{N110C} upregulation in the nervous system of mutant SOD1^{G37R} mice after disease onset reduces misfolded SOD1 accumulation and rescues spinal motor neurons

(A and F) Immunofluorescence staining of the ventral region of the lumbar spinal cord at the end stage (A) or symptomatic stage (F) of the disease stained for MNs (ChAT, white) and misfolded SOD1 (B8H10, red).

(B and G) Quantification of misfolded SOD1 intensity in the ventral horn of the lumbar spinal cord at disease end-stage ($n = 4$) (B) or symptomatic stage ($n = 3$) (G), normalized to GFP-treated group ($n = 4$) or to non-injected group ($n = 3$).

(C and H) Numerical quantification of ChAT-positive neurons in the ventral horn of the lumbar spinal cord at disease end-stage ($n = 4$) (C) or symptomatic stage ($n = 3$) (H), normalized to GFP-treated group or to non-injected group.

(D) Immunoprecipitation using B8H10 antibody to detect misfolded SOD1 in the lumbar spinal cord of GFP-, MIF-, or MIF^{N110C}-treated SOD1^{G37R} mice.

(E) Quantification of the bound misfolded SOD1 normalized to the level of endogenous SOD1 (mSOD1) ($n = 4$). Graphs represent mean ± SEM. Statistics were performed using one-way ANOVA followed by Tukey's multiple comparison test. Scale bars, 200, 100, and 50 μm. ****$p < 10^{-4}$,***$p < 10^{-3}$, **$p < 0.01$, *$p < 0.05$.

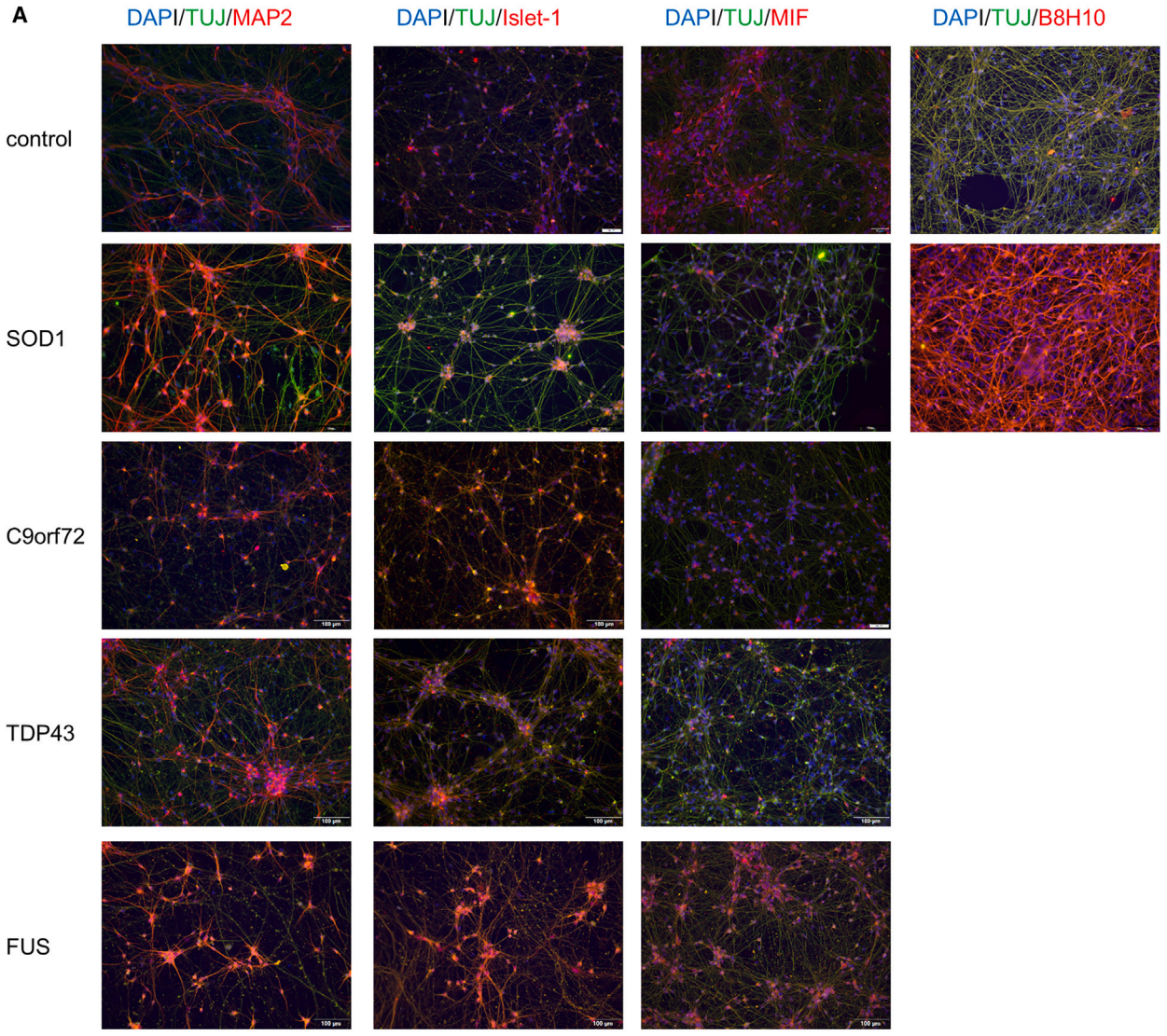

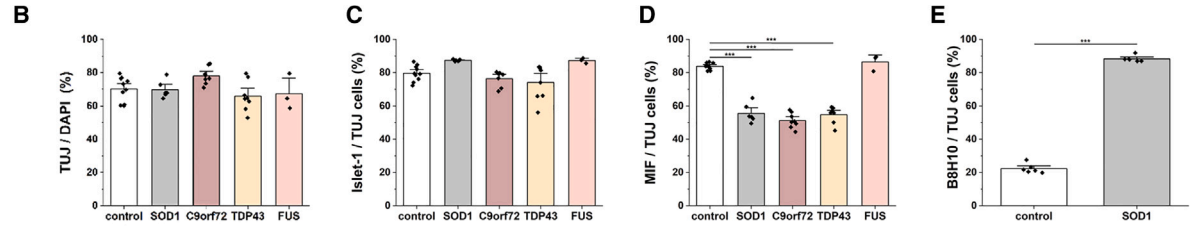

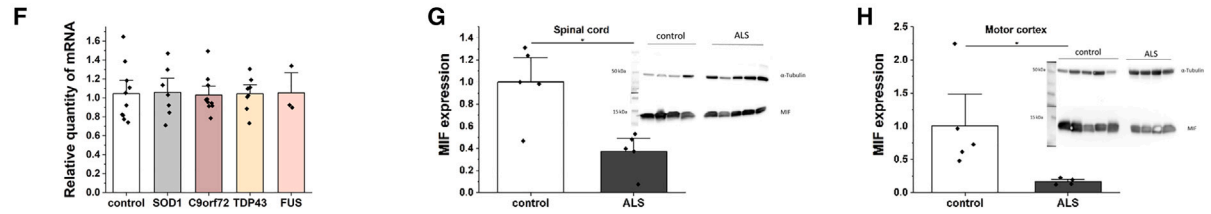

(legend on next page)

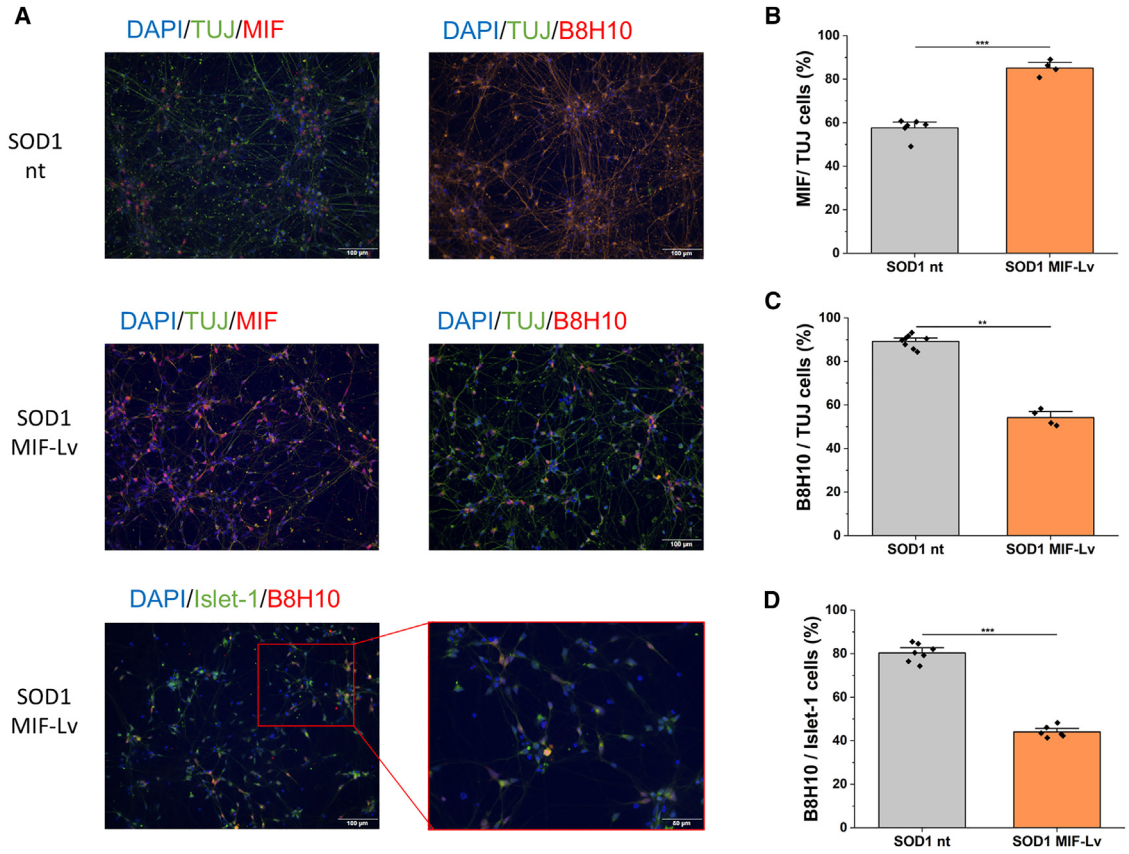

Figure 7. Lentiviral transduction of mutant SOD1 iPSC-derived motor neurons with MIF reduces SOD1 misfolding

(A) ICC staining for MIF and misfolded SOD1 before and after transduction of iPSC-derived mutant SOD1 MNs.

(B–D) Quantitative analysis of MIF and misfolded SOD1 protein expression in human IPSC-derived mutant SOD1 MNs. MIF expression (B) and misfolded SOD1 accumulation after MIF transduction in relation to TUJ-positive cells (C), and in relation to Islet-1-positive cells (D).>2 biological and >2 technical replicates. Graphs represent mean ± SEM. Statistics were performed using unpaired two-tailed t test. $^{**}p < 0.01$; $^{***}p < 0.001$); scale bars, 100 μm, 50 μm.

of animal models and their differences to human disease manifestation. Importantly, we also revealed low MIF protein levels in iPSC MNs derived from SOD1, TDP43, and C9orf72 cases. Additionally, we found that sporadic ALS patients, who have been reported to accumulate misfolded SOD1, according to several groups,[66–71] have lower MIF protein levels in the motor cortex and spinal cord. Therefore, low MIF protein levels found in familial and sporadic ALS patients might represent a common mechanism of MN vulnerability. Finally, MIF overexpression resulted in the reduction of misfolded SOD1 levels in iPSC-derived MNs from SOD1 patients, further confirming the relevance of this therapeutic concept. However, since this is an isolated *in vitro* system, we cannot rule out the involvement of other cell types in disease pathogenesis.

By using the AAV-PHP.eB viral system, we were able to express the human form of MIF, which is necessary, since the mutant SOD1 mice express the human transgene. Overexpression of MIF using the AAV-PHP.eB viral system allowed us to exploit all MIF's properties and functions, both the well studied as well as the ones yet to be investigated. If the observed beneficial effect was exclusively dependent on the binding of MIF to CD74 receptor, using an MIF agonist such as MIF020 that enhances MIF binding to the CD74 receptor,[72–74] might be more appropriate in the sense of avoiding an excess amount of MIF that may lead to unwanted side effects. The positive effect seen by both the WT form and the N110C mutant form of MIF, which retains only partial CD74 receptor binding activity and has impaired signaling ability as a cytokine,[23] however, suggests

Figure 6. Reduced MIF protein expression in ALS-patient-derived motor neurons and human ALS *post mortem* tissue

(A–E) Immunocytochemistry of typical neuronal (TUJ) and MN (Islet-1) markers, MIF, and misfolded SOD1 (B8H10) in human iPSC-derived control and ALS MNs after DIV 38. (D) $^{***}p < 0.001$, one-way ANOVA followed by Tukey's multiple comparison test; (E) $^{***}p < 0.001$, unpaired two-tailed t test.

(F) MIF mRNA expression of iPSC-derived MNs using RT-qPCR; scale bars, 100 μm.

(G and H) MIF expression normalized to α-tubulin in human *post mortem* tissue samples from spinal cord (G) or motor cortex (H) of sporadic ALS patients and healthy controls determined by immunoblots, n = 4–5; two or three technical replicates. Graphs represent mean ± SEM. Statistics were performed using Mann-Whitney U test or two-tailed t test. $^{*}p < 0.05$. See also Figure S8.

a different mechanism of action that does not depend only on the binding to CD74 receptor.

Fortunately for SOD1 familial ALS (fALS) patients, the intrathecally administered antisense oligonucleotide that reduces synthesis of the SOD1 protein[41,75,76] was recently approved by the US Food and Drug Administration (FDA). While downregulation of SOD1 can be effective in SOD1 fALS, its long-term effects must be carefully monitored so that the protein does not reach a critically low expression level,[77–79] and, for all other forms of fALS/sALS, efficient disease modifying therapies are urgently needed.

In summary, our findings shed light on the diverse roles of MIF in the CNS in general, and its importance in MNs specifically, when administered in a therapeutically relevant manner. MIF not only functions as a SOD1 chaperone that modulates SOD1 misfolding and aggregation but also affects diverse pathways, including the inflammatory response, neurogenesis, and metabolism, and results in better motor and neurological functions, leading to extended survival. Low MIF protein levels in MNs derived from iPSCs of SOD1 cases as well as C9orf72, TDP43, and the spinal cord of the sporadic patients, along with the *in vivo* results, opens avenues for its therapeutic potential for familial SOD1 ALS and ALS cases in general.

Limitations of the study

In this research, we used a human form of MIF to investigate its therapeutic effect on a mouse model of ALS (mice carrying human $SOD1^{G37R}$). However, as indicated by the results of RNA sequencing and proteomics, MIF's effect is not solely due to the inhibition of SOD1 misfolding and aggregation but also involves different pathways, including inflammation and neurogenesis. The activated pathways following MIF treatment are murine pathways that were activated by upregulation of human MIF. Thus, the effect of human MIF on those pathways needs to be verified in a human context.

STAR★METHODS

Detailed methods are provided in the online version of this paper and include the following:

SUPPLEMENTAL INFORMATION

Supplemental information can be found online at https://doi.org/10.1016/j.xcrm.2024.101546.

ACKNOWLEDGMENTS

This work was supported by grants from the Israel Science Foundation (ISF #284/19) to A.I. and German Israeli Foundation (GIF #I-116-415.6-2016) to A.I. and S.P. We thank the Answer ALS Consortium for the Answer ALS data. Also, we thank Dr. Meital Kupervaser, Dr. Hadas Keren-Shaul, and Dr. Tali Shalit from the Nancy and Stephen Grand Israel National Center for personalized medicine (G-INCPM), The Weizmann Institute, and Dr. Vered Chalifa-Caspi and Dr. Liron Levin from the Bioinformatics Core Facility, Ben Gurion University of the Negev. We also thank Dr. Essa Alfahel for his technical assistance.

We thank the Cellular and Molecular Digital Imaging Facility (CMDIF) platform of Dalhousie University for the training and access to the Zeiss LSM 880 confocal microscope.

AUTHOR CONTRIBUTIONS

Conceptualization, L.A, T.G., S.P., and A.I.; methodology, L.A., T.G., S.P., and A.I.; investigation, L.A., T.G., N.T., R.E.,V.K., L.D., R.G., A.K., K.B., and S.Z.; formal analysis, L.A. and T.G.; writing – original draft, L.A. and A.I.; writing – review & editing, L.A., T.G., V.K., L.D., R.G., A.K., K.B., J.K., V.R., E.F., N.S., J.V., S.P., and A.I.; funding acquisition, S.P. and A.I.; resources, J.S. and A.H.; supervision, A.I., S.P., T.C., and V.R.

DECLARATION OF INTERESTS

The authors declare no competing interests.

Received: May 17, 2023
Revised: November 3, 2023
Accepted: April 10, 2024
Published: May 3, 2024

REFERENCES

1. Bonafede, R., and Mariotti, R. (2017). ALS Pathogenesis and Therapeutic Approaches: The Role of Mesenchymal Stem Cells and Extracellular Vesicles. Front. Cell. Neurosci. *11*, 80.
2. Cleveland, D.W., and Rothstein, J.D. (2001). From Charcot to Lou Gehrig: deciphering selective motor neuron death in ALS. Nat. Rev. Neurosci. *2*, 806–819.
3. Da Cruz, S., and Cleveland, D.W. (2011). Understanding the role of TDP-43 and FUS/TLS in ALS and beyond. Curr. Opin. Neurobiol. *21*, 904–919.
4. Abu-Hamad, S., Kahn, J., Leyton-Jaimes, M.F., Rosenblatt, J., and Israelson, A. (2017). Misfolded SOD1 Accumulation and Mitochondrial Association Contribute to the Selective Vulnerability of Motor Neurons in Familial ALS: Correlation to Human Disease. ACS Chem. Neurosci. *8*, 2225–2234.

5. Wang, Q., Johnson, J.L., Agar, N.Y.R., and Agar, J.N. (2008). Protein aggregation and protein instability govern familial amyotrophic lateral sclerosis patient survival. PLoS Biol. *6*, e170.

6. Prudencio, M., Hart, P.J., Borchelt, D.R., and Andersen, P.M. (2009). Variation in aggregation propensities among ALS-associated variants of SOD1: correlation to human disease. Hum. Mol. Genet. *18*, 3217–3226.

7. Lukas, T.J., Luo, W.W., Mao, H., Cole, N., and Siddique, T. (2006). Informatics-assisted protein profiling in a transgenic mouse model of amyotrophic lateral sclerosis. Mol. Cell. Proteomics *5*, 1233–1244.

8. Israelson, A., Arbel, N., Da Cruz, S., Ilieva, H., Yamanaka, K., Shoshan-Barmatz, V., and Cleveland, D.W. (2010). Misfolded mutant SOD1 directly inhibits VDAC1 conductance in a mouse model of inherited ALS. Neuron *67*, 575–587.

9. Vande Velde, C., Miller, T.M., Cashman, N.R., and Cleveland, D.W. (2008). Selective association of misfolded ALS-linked mutant SOD1 with the cytoplasmic face of mitochondria. Proc. Natl. Acad. Sci. USA *105*, 4022–4027.

10. Israelson, A., Ditsworth, D., Sun, S., Song, S., Liang, J., Hruska-Plochan, M., McAlonis-Downes, M., Abu-Hamad, S., Zoltsman, G., Shani, T., et al. (2015). Macrophage migration inhibitory factor as a chaperone inhibiting accumulation of misfolded SOD1. Neuron *86*, 218–232.

11. Fujisawa, T., Homma, K., Yamaguchi, N., Kadowaki, H., Tsuburaya, N., Naguro, I., Matsuzawa, A., Takeda, K., Takahashi, Y., Goto, J., et al. (2012). A novel monoclonal antibody reveals a conformational alteration shared by amyotrophic lateral sclerosis-linked SOD1 mutants. Ann. Neurol. *72*, 739–749.

12. Nishitoh, H., Kadowaki, H., Nagai, A., Maruyama, T., Yokota, T., Fukutomi, H., Noguchi, T., Matsuzawa, A., Takeda, K., and Ichijo, H. (2008). ALS-linked mutant SOD1 induces ER stress- and ASK1-dependent motor neuron death by targeting Derlin-1. Genes Dev. *22*, 1451–1464.

13. Leyton-Jaimes, M.F., Kahn, J., and Israelson, A. (2018). Macrophage migration inhibitory factor: A multifaceted cytokine implicated in multiple neurological diseases. Exp. Neurol. *301*, 83–91.

14. Leyton-Jaimes, M.F., Benaim, C., Abu-Hamad, S., Kahn, J., Guetta, A., Bucala, R., and Israelson, A. (2016). Endogenous macrophage migration inhibitory factor reduces the accumulation and toxicity of misfolded SOD1 in a mouse model of ALS. Proc. Natl. Acad. Sci. USA *113*, 10198–10203.

15. Leyton-Jaimes, M.F., Kahn, J., and Israelson, A. (2019). AAV2/9-mediated overexpression of MIF inhibits SOD1 misfolding, delays disease onset, and extends survival in mouse models of ALS. Proc. Natl. Acad. Sci. USA *116*, 14755–14760.

16. Calandra, T., and Roger, T. (2003). Macrophage migration inhibitory factor: a regulator of innate immunity. Nat. Rev. Immunol. *3*, 791–800.

17. Roger, T., David, J., Glauser, M.P., and Calandra, T. (2001). MIF regulates innate immune responses through modulation of Toll-like receptor 4. Nature *414*, 920–924.

18. Kudrin, A., Scott, M., Martin, S., Chung, C.W., Donn, R., McMaster, A., Ellison, S., Ray, D., Ray, K., and Binks, M. (2006). Human macrophage migration inhibitory factor: a proven immunomodulatory cytokine? J. Biol. Chem. *281*, 29641–29651.

19. Kleemann, R., Kapurniotu, A., Frank, R.W., Gessner, A., Mischke, R., Flieger, O., Jüttner, S., Brunner, H., and Bernhagen, J. (1998). Disulfide analysis reveals a role for macrophage migration inhibitory factor (MIF) as thiol-protein oxidoreductase. J. Mol. Biol. *280*, 85–102.

20. Rosengren, E., Bucala, R., Aman, P., Jacobsson, L., Odh, G., Metz, C.N., and Rorsman, H. (1996). The immunoregulatory mediator macrophage migration inhibitory factor (MIF) catalyzes a tautomerization reaction. Mol. Med. *2*, 143–149.

21. Park, H., Kam, T.I., Peng, H., Chou, S.C., Mehrabani-Tabari, A.A., Song, J.J., Yin, X., Karuppagounder, S.S., Umanah, G.K., Rao, A.V.S., et al. (2022). PAAN/MIF nuclease inhibition prevents neurodegeneration in Parkinson's disease. Cell *185*, 1943–1959.e21.

22. Wang, Y., An, R., Umanah, G.K., Park, H., Nambiar, K., Eacker, S.M., Kim, B., Bao, L., Harraz, M.M., Chang, C., et al. (2016). A nuclease that mediates cell death induced by DNA damage and poly(ADP-ribose) polymerase-1. Science *354*, aad6872.

23. Fan, C., Rajasekaran, D., Syed, M.A., Leng, L., Loria, J.P., Bhandari, V., Bucala, R., and Lolis, E.J. (2013). MIF intersubunit disulfide mutant antagonist supports activation of CD74 by endogenous MIF trimer at physiologic concentrations. Proc. Natl. Acad. Sci. USA *110*, 10994–10999.

24. Shvil, N., Banerjee, V., Zoltsman, G., Shani, T., Kahn, J., Abu-Hamad, S., Papo, N., Engel, S., Bernhagen, J., and Israelson, A. (2018). MIF inhibits the formation and toxicity of misfolded SOD1 amyloid aggregates: implications for familial ALS. Cell Death Dis. *9*, 107.

25. Dayton, R.D., Grames, M.S., and Klein, R.L. (2018). More expansive gene transfer to the rat CNS: AAV PHP.EB vector dose-response and comparison to AAV PHP.B. Gene Ther. *25*, 392–400.

26. Chan, K.Y., Jang, M.J., Yoo, B.B., Greenbaum, A., Ravi, N., Wu, W.L., Sánchez-Guardado, L., Lois, C., Mazmanian, S.K., Deverman, B.E., and Gradinaru, V. (2017). Engineered AAVs for efficient noninvasive gene delivery to the central and peripheral nervous systems. Nat. Neurosci. *20*, 1172–1179.

27. Ge, S.X., Jung, D., and Yao, R. (2020). ShinyGO: a graphical gene-set enrichment tool for animals and plants. Bioinformatics *36*, 2628–2629.

28. Han, X., Wang, R., Zhou, Y., Fei, L., Sun, H., Lai, S., Saadatpour, A., Zhou, Z., Chen, H., Ye, F., et al. (2018). Mapping the Mouse Cell Atlas by Microwell-Seq. Cell *172*, 1091–1107.e17.

29. Schwartz, V., Krüttgen, A., Weis, J., Weber, C., Ostendorf, T., Lue, H., and Bernhagen, J. (2012). Role for CD74 and CXCR4 in clathrin-dependent endocytosis of the cytokine MIF. Eur. J. Cell Biol. *91*, 435–449.

30. Schwartz, V., Lue, H., Kraemer, S., Korbiel, J., Krohn, R., Ohl, K., Bucala, R., Weber, C., and Bernhagen, J. (2009). A functional heteromeric MIF receptor formed by CD74 and CXCR4. FEBS Lett. *583*, 2749–2757.

31. Jankauskas, S.S., Wong, D.W.L., Bucala, R., Djudjaj, S., and Boor, P. (2019). Evolving complexity of MIF signaling. Cell. Signal. *57*, 76–88.

32. Shi, X., Leng, L., Wang, T., Wang, W., Du, X., Li, J., McDonald, C., Chen, Z., Murphy, J.W., Lolis, E., et al. (2006). CD44 is the signaling component of the macrophage migration inhibitory factor-CD74 receptor complex. Immunity *25*, 595–606.

33. Wichmann, T.O., Damkier, H.H., and Pedersen, M. (2021). A Brief Overview of the Cerebrospinal Fluid System and Its Implications for Brain and Spinal Cord Diseases. Front. Hum. Neurosci. *15*, 737217.

34. Hor, J.H., Santosa, M.M., Lim, V.J.W., Ho, B.X., Taylor, A., Khong, Z.J., Ravits, J., Fan, Y., Liou, Y.C., Soh, B.S., and Ng, S.Y. (2021). ALS motor neurons exhibit hallmark metabolic defects that are rescued by SIRT3 activation. Cell Death Differ. *28*, 1379–1397.

35. Dupuis, L., Pradat, P.F., Ludolph, A.C., and Loeffler, J.P. (2011). Energy metabolism in amyotrophic lateral sclerosis. Lancet Neurol. *10*, 75–82.

36. Baxi, E.G., Thompson, T., Li, J., Kaye, J.A., Lim, R.G., Wu, J., Ramamoorthy, D., Lima, L., Vaibhav, V., Matlock, A., et al. (2022). Answer ALS, a large-scale resource for sporadic and familial ALS combining clinical and multi-omics data from induced pluripotent cell lines. Nat. Neurosci. *25*, 226–237.

37. Kwon, H.S., and Koh, S.H. (2020). Neuroinflammation in neurodegenerative disorders: the roles of microglia and astrocytes. Transl. Neurodegener. *9*, 42.

38. Boillée, S., Yamanaka, K., Lobsiger, C.S., Copeland, N.G., Jenkins, N.A., Kassiotis, G., Kollias, G., and Cleveland, D.W. (2006). Onset and progression in inherited ALS determined by motor neurons and microglia. Science *312*, 1389–1392.

39. Yamanaka, K., Chun, S.J., Boillee, S., Fujimori-Tonou, N., Yamashita, H., Gutmann, D.H., Takahashi, R., Misawa, H., and Cleveland, D.W. (2008).

Astrocytes as determinants of disease progression in inherited amyotrophic lateral sclerosis. Nat. Neurosci. *11*, 251–253.

40. Zaccai, S., Nemirovsky, A., Lerner, L., Alfahel, L., Eremenko, E., Israelson, A., and Monsonego, A. (2024). CD4 T-cell aging exacerbates neuroinflammation in a late-onset mouse model of amyotrophic lateral sclerosis. J. Neuroinflammation *21*, 17.
41. Miller, T., Cudkowicz, M., Shaw, P.J., Andersen, P.M., Atassi, N., Bucelli, R.C., Genge, A., Glass, J., Ladha, S., Ludolph, A.L., et al. (2020). Phase 1-2 Trial of Antisense Oligonucleotide Tofersen for SOD1 ALS. N. Engl. J. Med. *383*, 109–119.
42. Leone, P., Shera, D., McPhee, S.W.J., Francis, J.S., Kolodny, E.H., Bilaniuk, L.T., Wang, D.J., Assadi, M., Goldfarb, O., Goldman, H.W., et al. (2012). Long-term follow-up after gene therapy for canavan disease. Sci. Transl. Med. *4*, 165ra163.
43. Zhang, X., Chen, L., Wang, Y., Ding, Y., Peng, Z., Duan, L., Ju, G., Ren, Y., and Wang, X. (2013). Macrophage migration inhibitory factor promotes proliferation and neuronal differentiation of neural stem/precursor cells through Wnt/beta-catenin signal pathway. Int. J. Biol. Sci. *9*, 1108–1120.
44. Ohta, S., Misawa, A., Fukaya, R., Inoue, S., Kanemura, Y., Okano, H., Kawakami, Y., and Toda, M. (2012). Macrophage migration inhibitory factor (MIF) promotes cell survival and proliferation of neural stem/progenitor cells. J. Cell Sci. *125*, 3210–3220.
45. Conboy, L., Varea, E., Castro, J.E., Sakouhi-Ouertatani, H., Calandra, T., Lashuel, H.A., and Sandi, C. (2011). Macrophage migration inhibitory factor is critically involved in basal and fluoxetine-stimulated adult hippocampal cell proliferation and in anxiety, depression, and memory-related behaviors. Mol. Psychiatry *16*, 533–547.
46. Chai, X., Zhang, W., Li, L., Wu, Y., Zhu, X., and Zhao, S. (2020). Profile of MIF in Developing Hippocampus: Association With Cell Proliferation and Neurite Outgrowth. Front. Mol. Neurosci. *13*, 147.
47. Bendrat, K., Al-Abed, Y., Callaway, D.J., Peng, T., Calandra, T., Metz, C.N., and Bucala, R. (1997). Biochemical and mutational investigations of the enzymatic activity of macrophage migration inhibitory factor. Biochemistry *36*, 15356–15362.
48. Chiu, I.M., Chen, A., Zheng, Y., Kosaras, B., Tsiftsoglou, S.A., Vartanian, T.K., Brown, R.H., Jr., and Carroll, M.C. (2008). T lymphocytes potentiate endogenous neuroprotective inflammation in a mouse model of ALS. Proc. Natl. Acad. Sci. USA *105*, 17913–17918.
49. Contento, R.L., Molon, B., Boularan, C., Pozzan, T., Manes, S., Marullo, S., and Viola, A. (2008). CXCR4-CCR5: a couple modulating T cell functions. Proc. Natl. Acad. Sci. USA *105*, 10101–10106.
50. Haegel, H., Tölg, C., Hofmann, M., and Ceredig, R. (1993). Activated mouse astrocytes and T cells express similar CD44 variants. Role of CD44 in astrocyte/T cell binding. J. Cell Biol. *122*, 1067–1077.
51. Matsumoto, T., Imagama, S., Hirano, K., Ohgomori, T., Natori, T., Kobayashi, K., Muramoto, A., Ishiguro, N., and Kadomatsu, K. (2012). CD44 expression in astrocytes and microglia is associated with ALS progression in a mouse model. Neurosci. Lett. *520*, 115–120.
52. Morisaki, Y., Niikura, M., Watanabe, M., Onishi, K., Tanabe, S., Moriwaki, Y., Okuda, T., Ohara, S., Murayama, S., Takao, M., et al. (2016). Selective Expression of Osteopontin in ALS-resistant Motor Neurons is a Critical Determinant of Late Phase Neurodegeneration Mediated by Matrix Metalloproteinase-9. Sci. Rep. *6*, 27354.
53. Rabinovich-Nikitin, I., Ezra, A., Barbiro, B., Rabinovich-Toidman, P., and Solomon, B. (2016). Chronic administration of AMD3100 increases survival and alleviates pathology in SOD1(G93A) mice model of ALS. J. Neuroinflammation *13*, 123.
54. Rossi, D., Brambilla, L., Valori, C.F., Crugnola, A., Giaccone, G., Capobianco, R., Mangieri, M., Kingston, A.E., Bloc, A., Bezzi, P., and Volterra, A. (2005). Defective tumor necrosis factor-alpha-dependent control of astrocyte glutamate release in a transgenic mouse model of Alzheimer disease. J. Biol. Chem. *280*, 42088–42096.
55. Han, R., Liang, J., and Zhou, B. (2021). Glucose Metabolic Dysfunction in Neurodegenerative Diseases-New Mechanistic Insights and the Potential of Hypoxia as a Prospective Therapy Targeting Metabolic Reprogramming. Int. J. Mol. Sci. *22*, 5887.
56. Tefera, T.W., Steyn, F.J., Ngo, S.T., and Borges, K. (2021). CNS glucose metabolism in Amyotrophic Lateral Sclerosis: a therapeutic target? Cell Biosci. *11*, 14.
57. Kim, Y.J., Bond, G.J., Tsang, T., Posimo, J.M., Busino, L., and Brady, D.C. (2019). Copper chaperone ATOX1 is required for MAPK signaling and growth in BRAF mutation-positive melanoma. Metallomics *11*, 1430–1440.
58. Lan, Y.L., Wang, X., Lou, J.C., Xing, J.S., Zou, S., Yu, Z.L., Ma, X.C., Wang, H., and Zhang, B. (2018). Marinobufagenin inhibits glioma growth through sodium pump alpha1 subunit and ERK signaling-mediated mitochondrial apoptotic pathway. Cancer Med. *7*, 2034–2047.
59. Barwe, S.P., Anilkumar, G., Moon, S.Y., Zheng, Y., Whitelegge, J.P., Rajasekaran, S.A., and Rajasekaran, A.K. (2005). Novel role for Na,K-ATPase in phosphatidylinositol 3-kinase signaling and suppression of cell motility. Mol. Biol. Cell *16*, 1082–1094.
60. Chen, Y., Cai, T., Wang, H., Li, Z., Loreaux, E., Lingrel, J.B., and Xie, Z. (2009). Regulation of intracellular cholesterol distribution by Na/K-ATPase. J. Biol. Chem. *284*, 14881–14890.
61. Ou, W.B., Lundberg, M.Z., Zhu, S., Bahri, N., Kyriazoglou, A., Xu, L., Chen, T., Mariño-Enriquez, A., and Fletcher, J.A. (2021). YWHAE-NUTM2 oncoprotein regulates proliferation and cyclin D1 via RAF/MAPK and Hippo pathways. Oncogenesis *10*, 37.
62. Li, X., Wang, C., Wang, S., Hu, Y., Jin, S., Liu, O., Gou, R., Nie, X., Liu, J., and Lin, B. (2021). YWHAE as an HE4 interacting protein can influence the malignant behaviour of ovarian cancer by regulating the PI3K/AKT and MAPK pathways. Cancer Cell Int. *21*, 302.
63. Lue, H., Thiele, M., Franz, J., Dahl, E., Speckgens, S., Leng, L., Fingerle-Rowson, G., Bucala, R., Lüscher, B., and Bernhagen, J. (2007). Macrophage migration inhibitory factor (MIF) promotes cell survival by activation of the Akt pathway and role for CSN5/JAB1 in the control of autocrine MIF activity. Oncogene *26*, 5046–5059.
64. Bifulco, C., McDaniel, K., Leng, L., and Bucala, R. (2008). Tumor growth-promoting properties of macrophage migration inhibitory factor. Curr. Pharm. Des. *14*, 3790–3801.
65. Ren, Y., Chan, H.M., Li, Z., Lin, C., Nicholls, J., Chen, C.F., Lee, P.Y., Lui, V., Bacher, M., and Tam, P.K.H. (2004). Upregulation of macrophage migration inhibitory factor contributes to induced N-Myc expression by the activation of ERK signaling pathway and increased expression of interleukin-8 and VEGF in neuroblastoma. Oncogene *23*, 4146–4154.
66. Grad, L.I., Yerbury, J.J., Turner, B.J., Guest, W.C., Pokrishevsky, E., O'Neill, M.A., Yanai, A., Silverman, J.M., Zeineddine, R., Corcoran, L., et al. (2014). Intercellular propagated misfolding of wild-type Cu/Zn superoxide dismutase occurs via exosome-dependent and -independent mechanisms. Proc. Natl. Acad. Sci. USA *111*, 3620–3625.
67. Bosco, D.A., Morfini, G., Karabacak, N.M., Song, Y., Gros-Louis, F., Pasinelli, P., Goolsby, H., Fontaine, B.A., Lemay, N., McKenna-Yasek, D., et al. (2010). Wild-type and mutant SOD1 share an aberrant conformation and a common pathogenic pathway in ALS. Nat. Neurosci. *13*, 1396–1403.
68. Guareschi, S., Cova, E., Cereda, C., Ceroni, M., Donetti, E., Bosco, D.A., Trotti, D., and Pasinelli, P. (2012). An over-oxidized form of superoxide dismutase found in sporadic amyotrophic lateral sclerosis with bulbar onset shares a toxic mechanism with mutant SOD1. Proc. Natl. Acad. Sci. USA *109*, 5074–5079.
69. Medinas, D.B., Rozas, P., Martínez Traub, F., Woehlbier, U., Brown, R.H., Bosco, D.A., and Hetz, C. (2018). Endoplasmic reticulum stress leads to accumulation of wild-type SOD1 aggregates associated with sporadic amyotrophic lateral sclerosis. Proc. Natl. Acad. Sci. USA *115*, 8209–8214.

70. Forsberg, K., Andersen, P.M., Marklund, S.L., and Brännström, T. (2011). Glial nuclear aggregates of superoxide dismutase-1 are regularly present in patients with amyotrophic lateral sclerosis. Acta Neuropathol. *121*, 623–634.

71. Paré, B., Lehmann, M., Beaudin, M., Nordström, U., Saikali, S., Julien, J.P., Gilthorpe, J.D., Marklund, S.L., Cashman, N.R., Andersen, P.M., et al. (2018). Misfolded SOD1 pathology in sporadic Amyotrophic Lateral Sclerosis. Sci. Rep. *8*, 14223.

72. Jorgensen, W.L., Gandavadi, S., Du, X., Hare, A.A., Trofimov, A., Leng, L., and Bucala, R. (2010). Receptor agonists of macrophage migration inhibitory factor. Bioorg. Med. Chem. Lett. *20*, 7033–7036.

73. Leng, L., Chen, L., Fan, J., Greven, D., Arjona, A., Du, X., Austin, D., Kashgarian, M., Yin, Z., Huang, X.R., et al. (2011). A small-molecule macrophage migration inhibitory factor antagonist protects against glomerulonephritis in lupus-prone NZB/NZW F1 and MRL/lpr mice. J. Immunol. *186*, 527–538.

74. Yoo, S.A., Leng, L., Kim, B.J., Du, X., Tilstam, P.V., Kim, K.H., Kong, J.S., Yoon, H.J., Liu, A., Wang, T., et al. (2016). MIF allele-dependent regulation of the MIF coreceptor CD44 and role in rheumatoid arthritis. Proc. Natl. Acad. Sci. USA *113*, E7917–E7926.

75. Benatar, M., Wuu, J., Andersen, P.M., Bucelli, R.C., Andrews, J.A., Otto, M., Farahany, N.A., Harrington, E.A., Chen, W., Mitchell, A.A., et al. (2022). Design of a Randomized, Placebo-Controlled, Phase 3 Trial of Tofersen Initiated in Clinically Presymptomatic SOD1 Variant Carriers: the ATLAS Study. Neurotherapeutics *19*, 1248–1258.

76. Miller, T.M., Cudkowicz, M.E., Genge, A., Shaw, P.J., Sobue, G., Bucelli, R.C., Chiò, A., Van Damme, P., Ludolph, A.C., Glass, J.D., et al. (2022). Trial of Antisense Oligonucleotide Tofersen for SOD1 ALS. N. Engl. J. Med. *387*, 1099–1110.

77. Park, J.H., Nordström, U., Tsiakas, K., Keskin, I., Elpers, C., Mannil, M., Heller, R., Nolan, M., Alburaiky, S., Zetterström, P., et al. (2023). The motor system is exceptionally vulnerable to absence of the ubiquitously expressed superoxide dismutase-1. Brain Commun. *5*, fcad017.

78. Park, J.H., Elpers, C., Reunert, J., McCormick, M.L., Mohr, J., Biskup, S., Schwartz, O., Rust, S., Grüneberg, M., Seelhöfer, A., et al. (2019). SOD1 deficiency: a novel syndrome distinct from amyotrophic lateral sclerosis. Brain *142*, 2230–2237.

79. Ezer, S., Daana, M., Park, J.H., Yanovsky-Dagan, S., Nordström, U., Basal, A., Edvardson, S., Saada, A., Otto, M., Meiner, V., et al. (2022). Infantile SOD1 deficiency syndrome caused by a homozygous SOD1 variant with absence of enzyme activity. Brain *145*, 872–878.

80. Eggenschwiler, R., Gschwendtberger, T., Felski, C., Jahn, C., Langer, F., Sterneckert, J., Hermann, A., Lühmann, J., Steinemann, D., Haase, A., et al. (2021). A selectable all-in-one CRISPR prime editing piggyBac transposon allows for highly efficient gene editing in human cell lines. Sci. Rep. *11*, 22154.

81. Reinhardt, P., Glatza, M., Hemmer, K., Tsytsyura, Y., Thiel, C.S., Höing, S., Moritz, S., Parga, J.A., Wagner, L., Bruder, J.M., et al. (2013). Derivation and expansion using only small molecules of human neural progenitors for neurodegenerative disease modeling. PLoS One *8*, e59252.

82. Reinhardt, P., Schmid, B., Burbulla, L.F., Schöndorf, D.C., Wagner, L., Glatza, M., Höing, S., Hargus, G., Heck, S.A., Dhingra, A., et al. (2013). Genetic correction of a LRRK2 mutation in human iPSCs links parkinsonian neurodegeneration to ERK-dependent changes in gene expression. Cell Stem Cell *12*, 354–367.

83. Naujock, M., Stanslowsky, N., Bufler, S., Naumann, M., Reinhardt, P., Sterneckert, J., Kefalakes, E., Kassebaum, C., Bursch, F., Lojewski, X., et al. (2016). 4-Aminopyridine Induced Activity Rescues Hypoexcitable Motor Neurons from Amyotrophic Lateral Sclerosis Patient-Derived Induced Pluripotent Stem Cells. Stem Cell. *34*, 1563–1575.

84. Scekic-Zahirovic, J., Oussini, H.E., Mersmann, S., Drenner, K., Wagner, M., Sun, Y., Allmeroth, K., Dieterlé, S., Sinniger, J., Dirrig-Grosch, S., et al. (2017). Motor neuron intrinsic and extrinsic mechanisms contribute to the pathogenesis of FUS-associated amyotrophic lateral sclerosis. Acta Neuropathol. *133*, 887–906.

85. Kreiter, N., Pal, A., Lojewski, X., Corcia, P., Naujock, M., Reinhardt, P., Sterneckert, J., Petri, S., Wegner, F., Storch, A., and Hermann, A. (2018). Age-dependent neurodegeneration and organelle transport deficiencies in mutant TDP43 patient-derived neurons are independent of TDP43 aggregation. Neurobiol. Dis. *115*, 167–181.

86. Sivadasan, R., Hornburg, D., Drepper, C., Frank, N., Jablonka, S., Hansel, A., Lojewski, X., Sterneckert, J., Hermann, A., Shaw, P.J., et al. (2016). C9ORF72 interaction with cofilin modulates actin dynamics in motor neurons. Nat. Neurosci. *19*, 1610–1618.

87. Donnelly, C.J., Zhang, P.W., Pham, J.T., Haeusler, A.R., Mistry, N.A., Vidensky, S., Daley, E.L., Poth, E.M., Hoover, B., Fines, D.M., et al. (2013). RNA toxicity from the ALS/FTD C9ORF72 expansion is mitigated by antisense intervention. Neuron *80*, 415–428.

88. Love, M.I., Huber, W., and Anders, S. (2014). Moderated estimation of fold change and dispersion for RNA-seq data with DESeq2. Genome Biol. *15*, 550.

89. Schneider, C.A., Rasband, W.S., and Eliceiri, K.W. (2012). NIH Image to ImageJ: 25 years of image analysis. Nat. Methods *9*, 671–675.

90. Ewels, P., Magnusson, M., Lundin, S., and Käller, M. (2016). MultiQC: summarize analysis results for multiple tools and samples in a single report. Bioinformatics *32*, 3047–3048.

91. Tyanova, S., Temu, T., Sinitcyn, P., Carlson, A., Hein, M.Y., Geiger, T., Mann, M., and Cox, J. (2016). The Perseus computational platform for comprehensive analysis of (prote)omics data. Nat. Methods *13*, 731–740.

92. Li, B., and Dewey, C.N. (2011). RSEM: accurate transcript quantification from RNA-Seq data with or without a reference genome. BMC Bioinf. *12*, 323.

93. Dobin, A., Davis, C.A., Schlesinger, F., Drenkow, J., Zaleski, C., Jha, S., Batut, P., Chaisson, M., and Gingeras, T.R. (2013). STAR: ultrafast universal RNA-seq aligner. Bioinformatics *29*, 15–21.

94. Bairoch, A., and Apweiler, R. (1997). The SWISS-PROT protein sequence data bank and its supplement TrEMBL. Nucleic Acids Res. *25*, 31–36.

95. Perez-Riverol, Y., Bai, J., Bandla, C., García-Seisdedos, D., Hewapathirana, S., Kamatchinathan, S., Kundu, D.J., Prakash, A., Frericks-Zipper, A., Eisenacher, M., et al. (2022). The PRIDE database resources in 2022: a hub for mass spectrometry-based proteomics evidences. Nucleic Acids Res. *50*, D543–D552.

96. Faul, F., Erdfelder, E., Buchner, A., and Lang, A.G. (2009). Statistical power analyses using G*Power 3.1: tests for correlation and regression analyses. Behav. Res. Methods *41*, 1149–1160.

97. Faul, F., Erdfelder, E., Lang, A.G., and Buchner, A. (2007). G*Power 3: a flexible statistical power analysis program for the social, behavioral, and biomedical sciences. Behav. Res. Methods *39*, 175–191.

98. Bursch, F., Kalmbach, N., Naujock, M., Staege, S., Eggenschwiler, R., Abo-Rady, M., Japtok, J., Guo, W., Hensel, N., Reinhardt, P., et al. (2019). Altered calcium dynamics and glutamate receptor properties in iPSC-derived motor neurons from ALS patients with C9orf72, FUS, SOD1 or TDP43 mutations. Hum. Mol. Genet. *28*, 2835–2850.

99. Hatzipetros, T., Kidd, J.D., Moreno, A.J., Thompson, K., Gill, A., and Vieira, F.G. (2015). A Quick Phenotypic Neurological Scoring System for Evaluating Disease Progression in the SOD1-G93A Mouse Model of ALS. J. Vis. Exp. *104*, 53257. https://doi.org/10.3791/53257.

100. Deacon, R.M. (2013). Measuring the strength of mice. J. Vis. Exp *76*, 2610. https://doi.org/10.3791/2610.

101. Challis, R.C., Ravindra Kumar, S., Chan, K.Y., Challis, C., Beadle, K., Jang, M.J., Kim, H.M., Rajendran, P.S., Tompkins, J.D., Shivkumar, K., et al. (2019). Systemic AAV vectors for widespread and targeted gene delivery in rodents. Nat. Protoc. *14*, 379–414.

102. Baruch, K., Kertser, A., Porat, Z., and Schwartz, M. (2015). Cerebral nitric oxide represses choroid plexus NFkappaB-dependent gateway activity for leukocyte trafficking. EMBO J. *34*, 1816–1828.

103. Sklarz, M., Levin, L., Gordon, M., and Chalifa-Caspi, V. (2018). NeatSeq-Flow: A Lightweight High-Throughput Sequencing Workflow Platform for Non-pProgrammers and Programmers Alike. bioRxiv. https://doi.org/10.1101/173005.

104. Röst, H.L., Rosenberger, G., Navarro, P., Gillet, L., Miladinović, S.M., Schubert, O.T., Wolski, W., Collins, B.C., Malmström, J., Malmström, L., and Aebersold, R. (2014). OpenSWATH enables automated, targeted analysis of data-independent acquisition MS data. Nat. Biotechnol. *32*, 219–223.

105. Rost, H.L., Liu, Y., D'Agostino, G., Zanella, M., Navarro, P., Rosenberger, G., Collins, B.C., Gillet, L., Testa, G., Malmstrom, L., and Aebersold, R. (2016). TRIC: an automated alignment strategy for reproducible protein quantification in targeted proteomics. Nat. Methods *13*, 777–783.

106. Zhang, Y., Parmigiani, G., and Johnson, W.E. (2020). ComBat-seq: batch effect adjustment for RNA-seq count data. NAR Genom. Bioinform. *2*, lqaa078.

107. Cleveland, W.S., Grosse, E., and Shyu, W.M. (2017). Local regression models. In Statistical models in S (Routledge), pp. 309–376.

108. Sundararaman, N., Bhat, A., Venkatraman, V., Binek, A., Dwight, Z., Ariyasinghe, N.R., Escopete, S., Joung, S.Y., Cheng, S., Parker, S.J., et al. (2023). BIRCH: An Automated Workflow for Evaluation, Correction, and Visualization of Batch Effect in Bottom-Up Mass Spectrometry-Based Proteomics Data. J. Proteome Res. *22*, 471–481.

109. Teo, G., Kim, S., Tsou, C.C., Collins, B., Gingras, A.C., Nesvizhskii, A.I., and Choi, H. (2015). mapDIA: Preprocessing and statistical analysis of quantitative proteomics data from data independent acquisition mass spectrometry. J. Proteomics *129*, 108–120.

STAR★METHODS

KEY RESOURCES TABLE

REAGENT or RESOURCE	SOURCE	IDENTIFIER
Antibodies		
α-bungarotoxin (BTX) conjugated to rhodamine	Invitrogen	Molecular Probes Cat# T1175, RRID:AB_2313931
Alexa Fluor 488 goat anti-mouse IgG	Invitrogen	Thermo Fisher Scientific Cat# A-21121, RRID:AB_2535764
Alexa Fluor 555 goat anti-mouse IgG1	Invitrogen	Thermo Fisher Scientific Cat# A-21127, RRID:AB_2535769
Alexa Fluor 488 goat anti-mouse IgG2a	Invitrogen	Thermo Fisher Scientific Cat# A-21131, RRID:AB_2535771
Alexa Fluor 488 goat anti-rabbit IgG	Invitrogen	Thermo Fisher Scientific Cat# A-11008, RRID:AB_143165
Alexa Fluor 555 donkey anti-mouse IgG	Invitrogen	Thermo Fisher Scientific Cat# A-31570, RRID:AB_2536180
Alexa Fluor 555 donkey anti-rabbit IgG	Invitrogen	Thermo Fisher Scientific Cat# A-31572, RRID:AB_162543
Alexa Fluor 633 goat anti-Rat IgG	Invitrogen	Thermo Fisher Scientific Cat# A-21094, RRID:AB_2535749
Alexa Fluor 647 chicken anti-rabbit IgG	Invitrogen	Thermo Fisher Scientific Cat# A-21443, RRID:AB_2535861
Alexa Fluor 647 donkey anti-goat IgG	Abcam	Abcam Cat# ab150135, RRID:AB_2687955
Alexa Fluor 647 goat anti-rabbit IgG	Invitrogen	Thermo Fisher Scientific Cat# A-21244, RRID:AB_2535812
Anti-CD3	BioLegend	BioLegend Cat# 100301 (also 100302), RRID:AB_312666
Anti-CD4	BioLegend	BioLegend Cat# 100505 (also 100506), RRID:AB_312708
anti- SV2	DSHB	DSHB Cat# SV2, RRID:AB_2315387
anti-Choline Acetyltransferase	Merck	Millipore Cat# AB144P, RRID:AB_2079751
anti-Choline Acetyltransferase	Genetex	GeneTex Cat# GTX113164, RRID:AB_1949973
anti-GFAP	Merck	Millipore Cat# MAB360, RRID:AB_11212597
anti-HA	Abcam	Abcam Cat# ab9110, RRID:AB_307019
anti-Iba1	Abcam	Abcam Cat# ab5076, RRID:AB_2224402
anti-Iba1	Abcam	Abcam Cat# ab178846, RRID:AB_2636859
anti-SOD1	santa-cruz	Santa Cruz Biotechnology Cat# sc-101523, RRID:AB_2191632
anti-β III Tubulin	Abcam	Abcam Cat# ab18207, RRID:AB_444319
Anti-B8H10	Medi-mabs	MediMabs Cat# MM-0070-P, RRID:AB_2909641
Anti-MIF	Abcam	Abcam Cat#ab187064, RRID:AB_2934299
Anti-α-Tubulin	Santa-cruz	Santa Cruz Biotechnology Cat# sc-32293, RRID:AB_628412
anti-β III Tubulin mouse	Abcam	Abcam Cat#78078, RRID:AB_2256751
Anti-Map2	Abcam	Abcam Cat#ab32454, RRID:AB_776174
Anti-Islet1	Abcam	Abcam Cat#ab20670, RRID:AB_881306
Cy3 Goat Anti-Armenian Hamster IgG	Jackson ImmunoResearch Labs	Jackson ImmunoResearch Labs Cat# 127-165-160, RRID:AB_2338989

(*Continued on next page*)

Continued

REAGENT or RESOURCE	SOURCE	IDENTIFIER
Rabbit IgG Horseradish Peroxidase-conjugated Antibody	R&D Systems	R and D Systems Cat# HAF008, RRID:AB_357235
Mouse IgG Horseradish Peroxidase-conjugated Antibody	R&D Systems	R and D Systems Cat# HAF007, RRID:AB_357234
Bacterial and virus strains		
AAV-PHP.eB eGFP	This paper	N/A
AAV-PHP.eB MIF$^{N11\circ C}$ -HA	This paper	N/A
AAV-PHP.eB MIF^{WT}	This paper	N/A
Lenti CAG MIF-IRES-mKO2	This paper	N/A
Lenti CKO2AP	Eggenschwiler et al.[80]	N/A
Biological samples		
Postmortem tissue (motor cortex, spinal cord) from sporadic ALS patients and healthy patients with no evidence of neurologic or psychiatric disease	Autopsies. See Table S4.	N/A
Chemicals, peptides, and recombinant proteins		
Benzonase	Sigma	E1014-5KU
Dynabeads^{TM} protein G	Invitrogen	Dy-10004D
Fast SYBR green	Applied Biosystems	4385612
OptiPrep	Sigma	D1556
PFA	Sigma	441244
Poloxamer 188 solution (Pluronic-F68)	Sigma	P5556
Polyethylene Glycol (PEG) Bioultra 8000 250G	Sigma	89510-250G-F
Matrigel	Corning	Cat# 354234
Accutase	Gibco	A11105-01
poly-DL-ornithine-hydrobromide	Sigma-Aldrich/Merck	P8638
Laminin (mouse)	Gibco	Cat#23017-015
CHIR 99201	Axon Medchem	Cat# 1386
Purmorphamine	Cayman Chemical	Cat#10009634
Smoothened Agonist	Cayman Chemical	Cat# 11914
Retinoic acid	Sigma	R2625
BDNF	Peprotech	Cat# 450-02
GDNF	Peprotech	Cat# 450-10
dbcAMP	Sigma Aldrich/Merck,	D0260
Mowiol	Roth	Cat# 0713.1
NEBuilder® HiFi DNA Assembly Master Mix	NEB	NEB E2621L
Phusion^{TM} Hot Start II High-Fidelity DNA-Polymerase	Thermo Fisher Scientific	Cat# F549L
Critical commercial assays		
RNeasy plus mini kit	Qiagen	74134
RNeasy Mini Kit	Qiagen	74104
Pierce BCA Protein-Assay kit	Thermo Scientific	Cat# 23227
SuperSignal West Pico PLUS	Thermo Scientific	Cat# 34577
Experimental models: Cell lines		
HEK-293T cells	ATCC	RRID:CVCL_4V93
Healthy Control #1 cell line	Reinhardt et al.[81] Reinhardt et al.[82]	N/A
Healthy Control #2 cell line	Reinhardt et al.[81] Reinhardt et al.[82]	N/A

(*Continued on next page*)

Continued

REAGENT or RESOURCE	SOURCE	IDENTIFIER
Healthy Control #3 cell line	Naujock et al.[83]	N/A
FUS cell line	Naujock et al.[83] Scekic-Zahirovic et al.[84]	N/A
SOD1 #1 cell line	Naujock et al.[83]	N/A
SOD1 #2 cell line	Naujock et al.[83]	N/A
TDP43 #1 cell line	Kreiter et al.[85]	N/A
TDP43 #2 cell line	Kreiter et al.[85]	N/A
C9orf72 #1 cell line	Sivadasan et al.[86]	N/A
C9orf72 #2 cell line	Sivadasan et al.[86]	N/A
C9orf72 #3 cell line	Donnelly et al.[87]	N/A
Experimental models: Organisms/strains		
LoxSOD1^{G37R} mice	Jackson Laboratory	RRID:IMSR_JAX:016149
B6.Cg-Tg(SOD1*G93A)1Gur/J	Jackson Laboratory	RRID:IMSR_JAX:004435
Oligonucleotides		
Oligonucleotides	See Table S2.	N/A
Recombinant DNA		
pAAV-CAG-GFP	Addgene	RRID:Addgene_37825
pAAV-CAG-MIF-HA	This paper	N/A
pAAV-CAG- MIF$^{N11\circ}$C -HA	This paper	N/A
pAdDeltaF6	Addgene	RRID:Addgene_112867
pUCmini-iCAP-PHP.eB	Addgene	RRID:Addgene_103005
Software and algorithms		
cutadapt (v1.15)	Read the Docs	https://cutadapt.readthedocs.io/en/stable/
DESeq2[53] R package	Love et al.[88]	https://bioconductor.org/packages/release/bioc/html/DESeq2.html
FASTQC (v0.11.8)	Babraham Institute	https://www.bioinformatics.babraham.ac.uk/projects/
ImageJ software	Schneider et al.[89]	https://imagej.net/ij/index.html
MultiQC (v1.0.dev0)	Ewels et al.[90]	https://github.com/ewels/MultiQC
NIS-elements software	Nikon	https://www.microscope.healthcare.nikon.com/products/software/nis-elements
Originlab Pro	OriginLab Corporation	https://www.originlab.com/
Perseus v1.6.2.3. Decoy	Tyanova et al.[91]	https://maxquant.net/perseus/
RSEM (v1.2.28)	Li et al.[92]	http://deweylab.biostat.wisc.edu/rsem
ShinyGO	Ge et al.[27]	http://bioinformatics.sdstate.edu/go/
STAR (v2.5.2a)	Dobin et al.[93]	http://code.google.com/p/rna-star/
SVA/Combat R package	R Bioconductor	https://bioconductor.org/packages/release/bioc/html/sva.html
SwissProt proteome database	Bairoch et al.[94]	https://www.uniprot.org/uniprotkb?query=reviewed:true
Trim Galore (v0.4.5)	Babraham Institute	http://www.bioinformatics.babraham.ac.uk/projects/trim_galore.
QuantStudio Real-Time PCR Software	Thermo Fisher	https://www.thermofisher.com/de/de/home/global/forms/life-science/quantstudio-6-7-flex-software.html
Chemilumineszenz Imager	Intas Science Instruments, Gottingen, Germany	N/A
LabImage1D	Intas Science Instruments, Gottingen, Germany	N/A

(*Continued on next page*)

Continued

REAGENT or RESOURCE	SOURCE	IDENTIFIER
Olympus CellSens Dimension (v.1.18)	Olympus, Hamburg, Germany	https://www.olympus-lifescience.com/en/software/cellsens/?creative=651972827940&keyword=olympus%20cellsens%20dimension&matchtype=e&network=g&device=c&campaignid=19865307548&adgroupid=144087470581&gclid=EAIaIQobChMIr_m09IuJ_wIVTeLVCh2MnwKpEAAYASAAEgKWcvD_BwE
G*power software	University of Düsseldorf, Germany	https://www.gpower.hhu.de
Deposited data		
Mice RNA sequencing data	GEO	GSE246397
Mice CSF proteomics data	PRIDE	PXD046619
Answer ALS iPSC-derived MNs proteomics	Answer ALS Consortium	dataportal.answerals.org

RESOURCE AVAILABILITY

Lead contact

Further information and requests for resources and reagents should be directed to and will be fulfilled by the lead contact, Adrian Israelson (adriani@bgu.ac.il).

Materials availability

This study did not generate new unique reagents.

Data and code availability

- Data: RNA-seq data and CSF proteomics data have been deposited at GEO and PRIDE, accordingly, and are publicly available as of the date of publication. The RNA-seq data have been deposited to the GEO repository with accession number GSE246397. The mass spectrometry proteomics data have been deposited to the ProteomeXchange Consortium via the PRIDE[95] partner repository with the dataset identifier PXD046619 and https://doi.org/10.6019/PXD046619. Accession numbers are also listed in the key resources table. A large portion of the Answer ALS iPSC-derived MNs proteomics data used in this study is currently publicly available through the Answer ALS Data Portal (https://dataportal.answerals.org) following approval of a Data Use Agreement (DUA) form. However, all data and code used in this study will be made available by request to the lead contact following DUA approval.
- Code: This study did not generate any code.
- Any additional information required to reanalyze the data reported in this work paper is available from the lead contact upon request.

EXPERIMENTAL MODEL AND SUBJECT DETAILS

Mice

Female and male loxSOD1^{G37R} mice[38] were monitored weekly from the age of 160 days (before the disease onset), and subsequently, at the age of 210 days (disease onset), they were injected with AAV-PHP.eB eGFP, AAV-PHP.eB MIF^{WT}, or AAV-PHP.eB MIF$^{N11\circ C}$ into the tail vein. The mice were maintained in Ben-Gurion University of the Negev animal facility, and all procedures were approved by the animal care and use committee of Ben-Gurion University of the Negev and according to Israel's Animal Welfare Act 1994 and follows the Guide for Care and Use of Laboratory Animals (NRC 2011). Housing conditions are: 12:12 light:dark cycles at 20°C–24°C and 30–70% relative humidity. Mice are free fed autoclaved rodent chow, have free access to reverse osmosis filtered water, and are housed in individually ventilated cages.

Post hoc power analysis of survival study

A post hoc power analysis was performed for the statistical evaluation of the SOD1^{G37R} mice survival study and resulted in an achieved power of 80%. The analyses were performed with the G*power software[96,97] using the achieved significance of 0.01, a total group size of 47 mice and an effect size of 0.57 calculated from the mean values. For the calculation of the effect size, the three groups to be compared were used with a mean standard deviation of 21.17 and the following mean values and group sizes: Group 1 (SOD1^{G37R} untreated mice): n = 14, mean = 397.92; Group 2 (MIF treated SOD1^{G37R} mice): n = 16, mean = 425.25; Group 3 (MIF^{N110C} treated SOD1^{G37R} mice): n = 17, mean = 423.65.

SmNPCs and MN differentiation

All used small molecular neural progenitor cell lines (smNPC) are listed in Table S3. Cultivation of smNPCs and motor neuron (MN) differentiation was done as previously described.[83,98] Shortly, all smNPCs were maintained in N2B27 media supplemented with 150 μM ascorbic acid, 3 μM CHIR 99201 and 0.5 μM PMA. At least once a week smNPC lines were passaged in a 1:8-10 ratio using accutase (Life Technologies, Darmstadt, Germany) for up to 4 min at 37°C and replated onto matrigel (Corning, Corning, USA)-coated 6-well plates. MN differentiation was started by substituting the aforementioned supplements first with 1μM SAG for 4 days, 1μM RA, 0.5μM SAG, 5 ng/mL BDNF and 5 ng/mL GDNF for another 7 days. After 11 days of differentiation cells were detached using accutase and plated at a density of 1 × 10^6 cells/6-well and 3-5x10^5 cells/24-well with glass coverslips coated with poly-DL-ornithine-hydrobromide (0.5 mg/mL) and laminin (1 μg/mL, both Sigma-Aldrich/Merck, Darmstadt, Germany). Maturation of the patterned MNs was accomplished in N2-B27 media enriched with 150 μm ascorbic acid, 20 ng/mL BDNF, 20 ng/mL GDNF (both Peprotech, Hamburg, Germany) and 5 μm dbcAMP (Sigma Aldrich/Merck, Darmstadt, Germany) for another 28 days. After 38–40 days of MN differentiation cells on poly-DL-ornithine-hydrobromide/laminin coated 12 mm glass coverslips were analyzed by immunocytochemistry.

Human postmortem tissue

For analysis of spinal cord and motor cortex, human postmortem tissue of patients with a diagnosis of probable or definite sporadic ALS according to the El Escorial criteria and postmortem tissue of patients with no evidence of neurologic or psychiatric disease was collected (after informed consent by the patient or his/her relatives as approved by the ethics committee of Hannover Medical School) (Table S4). Samples of 6–7 ALS patients aged 44 to 77 years were compared with 4–5 controls aged 42 to 77 years by Western blot analyses.

METHOD DETAILS

Disease evaluation

All the mice were blindly evaluated once a week on the same day and hour by measuring weight, Neuroscore, grip strength, and hanging time.

Neuroscore

Briefly, as previously described.[99] NeuroScore evaluates mouse hindlimbs splay while the mouse is suspended from the tail, abnormal walking (including toe curl and foot-dragging), rigid paralysis in the hindlimb, minimal joint movement, and the ability of the mouse to right itself in 10 s upon placing it on either side. A higher NeuroScore indicates a more advanced motor dysfunction, and a Neuroscore of 4 indicates reaching the humane end-point.

Inverted screen test

This was used to measure hanging time. Briefly, as previously,[100] mice were placed in the middle of a grid screen and inverted within 2 s upside down above a padded surface. The hanging time was measured up to 60 s.

Grip strength test

The measures were obtained using the Chatillon DFE II series device, as described before.[15] Each mouse was measured 3 times, and the average was calculated.

Adeno-associated virus (AAV) production

Modified from.[101] Briefly, HEK-293T cells were seeded on 15 cm plates with 20 mL media [DMEM, 5% FBS, 2X nonessential amino acids, 2X Sodium pyruvate, 4mM L-glutamine, 100 units/ml Ampicillin, 0.1 mg/ml Streptomycin] and were incubated at 37°C, 5% CO2. Thirty six hours after seeding, cells were triple transfected with pAAV:capsid:pHelper plasmid to the ratio of 1:4:2 μg of DNA with a total amount of 40 μg per 150 mm dish (5.7 μg of pAAV, 22.8 μg of the capsid, and 11.4 μg of pHelper), using PEI transfection reagent. Following the transfection (12–24 h), the medium was replaced with 20 mL fresh enriched medium (10% FBS). After an additional 48 h, the medium was collected, stored at 4°C, and replaced with fresh medium. Following another 48 h, the cells were harvested using a cell scraper and transferred to collection tubes with the media. The tubes containing the cells and the media were centrifuged at 200 x g for 15 min. The supernatant and the stored media, were centrifuged at 2000 x g for 15 min at 4°C. Following centrifugation, the collected supernatant was incubated with 8% PEG solution for 2 h on ice. Parallelly, the pellet was lysed with 5 mL lysis virion buffer [150 mM NaCl, 50 mM Tris-HCl (pH 8.5)] and subjected to three rounds of freeze/thaw cycles, each round composed of 10 min in −80°C ethanol bath and then 10 min at 37°C followed by vertexing. Subsequently, 50 units of Benzonase per plate was added, and the lysate was incubated for 1.5 h at 37°C. The ice-incubated supernatant was centrifuged at 4,000 x g for 30 min at 4°C, and the pellet was lysed with a 5 mL lysis virion buffer and then added to the already handled lysate along with additional 10 units of Benzonase and left for an additional 30 min water bath incubation at 37°C. Finally, the lysate was centrifuged at 2,000 x g for 10 min at RT and filtered using a 0.45 μm filter. The crude lysate was stored at −80°C.

Capsid: pUCmini-iCAP-PHP.eB (plasmid #103005, Addgene), pHelper: pAdDeltaF6 (plasmid #112867, Addgene). Virion purification was accomplished using an OptiPrep density gradient. The crude lysate was loaded on the OptiPrep gradient (with a density of

60%, 40%, 25%, and 15%) and ultra-centrifuged at 200,000 x g for 2 h at 18°C. Subsequently, the viral fraction was collected from the 40/60% interface and the 40% layer. The collected fraction was then filtered using a 0.22 μm filter and transferred to an Amicon Ultra Centrifugal Filter with MWCO of 100 kDa, followed by washing with PBS containing 0.001% Pluronic-F68 by centrifugation at 3000 x g, 4°C. Following the final wash, where less than 300 μL of the solution was retained in the top chamber, the solution was filtered again using a 0.22 μm filter. The virion capsids were broken down to release the DNA for quantification. The virions were quantified by qPCR using SYBR green and primers targeting the WPRE region.

Each mouse was injected with 1.2 X 10^{14} vg/Kg, as the high dose described.[25]

Lentivirus production

Lentiviral vectors were produced by transient transfection of Lenti CAG-MIF-IRES-mKO2 or Lenti CKO2AP plasmids along with pCDNA3.GP.4xC, pMD2.G and pRSV-Rev into HEK293T cells using the CaCl2 protocol as described previously.[80] Vectors were titrated by transduction of serial-fold dilutions of 1:100–1:300,000 on HEK293T cells followed by FACS analysis 72 h post transduction. For generation of MIF-IRES-mKO2 or mKO2-T2A-PAC expressing bulk populations, 450,000 cells of control or ALS-SOD1 smNPC cell line were seeded per 6-well one day prior to transduction. Next day, culture medium was exchanged with medium supplemented with 8 μg/mL protamine sulfate (Sigma-Aldrich, Merck, Darmstadt, Germany) and cells were transduced at a calculated multiplicity of infection (MOI) of 1 with Lenti CAG-MIF-IRES-mKO2 or Lenti CKO2AP vector particles. Cells were expanded and FACS analyzed on day 13-post transduction, as well as on day 33 of MN differentiation, confirming continuous transgene expression during and after differentiation.

Tissue lysis and immunoblotting

Tissues were lysed mechanically in cold lysis buffer [50 mM Tris-HCl (pH 8.0), 150 mM NaCl, 1% NP-40, 1 mM PMSF, protease inhibitor x1 (Apex Bio)] by homogenization followed by further mechanical lysis through a 29G needle. The tissue lysate was incubated for 2 h on ice with agitation and afterward centrifuged for 20 min at 12,000 rpm, at 4°C. After preparing samples with sample buffer and boiling, the proteins were separated using 15 or 13% SDS-PAGE gel, transferred to a nitrocellulose membrane, and blocked for 1 h at room temperature with 5% milk, followed by overnight incubation at 4°C with primary antibody [mouse anti-SOD1 (1:1000, Santa-Cruz), rabbit anti-Iba (1:500, Abcam, UK), mouse anti-GFAP (1:1000, Merck), rabbit anti-HA (1:7,500, Abcam, UK), and mouse anti-GAPDH (1:500, Santa-Cruz)]. Following washing, the membranes were incubated for 1 h at room temperature with horseradish peroxidase-conjugated secondary antibody and subsequently detected by ECL (Biological industries or Cyanagen). Band intensity was quantified using ImageJ software.

Immunoprecipitation

B8H10 antibody was linked to Dynabeads protein G (Invitrogen, USA) for 1 h at room temperature. This was followed by incubating spinal cord extract (100 μg) in IP buffer [50 mM Tris-HCl (pH 7.4), 150 mM NaCl] together with the Dynabeads-antibody complex at 4°C overnight with agitation. The unbound fractions were separated from the Dynabeads-antibody-bound fraction complex and prepared for immunoblotting by adding sample buffer and boiling at 95°C for 5 min. Then, the beads with the bound fraction were washed 3 times with IP-washing buffer [50 mM Tris-HCl (pH 7.4), 0.5 M NaCl], and the bound fraction was eluted by adding sample buffer x2 and boiling at 95°C for 5 min.

Immunohistochemistry

Mice were anesthetized with Isoflurane and then perfused with cold 0.1 M PBS, followed by perfusion with 4% paraformaldehyde in 0.1 M PBS. The spinal cords were dissected and post-fixed in 4% formaldehyde in 0.1 M PBS at 4°C overnight, and then cryoprotected in 25% sucrose in 0.1 M PBS for 48 h at 4°C. Spinal cords were cryosectioned into 35 μm free-floating sections and blocked for 1 h in blocking solution (0.1 M PBS, 1% BSA, 10% secondary-antibody host serum, and 0.3% Triton X-100), followed by incubation overnight at 4°C with primary antibodies [goat anti-Choline Acetyltransferase (1:100, Merck, USA), rabbit anti-Choline Acetyltransferase (1:750, Genetex, USA), goat anti-Iba1 (1:500, Abcam, UK), mouse anti-GFAP (1:400, Merck. USA), rabbit anti-HA (1:500, Abcam, UK), mouse anti-B8H10 (1:100, MediMabs, Germany), Armenian hamster anti-CD3 (1:100, BioLegend, USA), and rat anti-CD4 (1:100, BioLegend, USA). Secondary antibodies used: Alexa Fluor 555 donkey anti-rabbit IgG (Invitrogen, USA), Alexa Fluor 555 donkey anti-mouse IgG (Invitrogen, USA), Alexa Fluor 647 chicken anti-Rabbit IgG (Invitrogen, USA), Alexa Fluor 647 donkey anti-goat IgG (Abcam, UK), Cy3 goat anti-Armenian hamster IgG (Jackson ImmunoResearch Labs, USA), and Alexa Fluor 633 goat anti-rat IgG (Invitrogen, USA)] diluted in 0.1M PBS containing 1% BSA, 1% secondary-antibody host serum, and 0.15% Triton X-100. Sections were subsequently washed three times in 0.1 M PBS with 0.003% tween and then incubated for 1.5 h at room temperature with fluorescently conjugated secondary antibodies. The sections were then washed 3 times with 0.1 M PBS. After immune mounting and allowing the slides to dry, images were acquired on a NIKON C2Plus laser unit dock to a Nikon Eclipse Ti unit of a confocal microscope using a 20X objective. Intensity quantification was performed using NIS-elements software.

CSF collection and proteomics

CSF was collected using cisterna magna puncture, as previously described.[102]

Briefly, mice were anesthetized with intraperitoneal Ketamine-xylazine injection and placed on a stereotactic frame with their head and body forming a 135° angle. The skin was cut sagittally inferior to the occiput, and the subcutaneous tissue and muscle were separated. A capillary was then inserted into the cisterna magna through the dura matter lateral to the arteria dorsalis spinalis. Approximately 10 μL CSF was collected from each mouse. The CSF was centrifuged at 15,000 x g for 30 s and checked for any blood contamination.

Later on, the CSF was subjected to in-solution tryptic digestion and desalting before being analyzed using nanoflow liquid chromatography (Acquity M-class) coupled to high resolution, high mass accuracy mass spectrometry (Fusion Lumos). Each sample was analyzed separately in a random order in discovery mode. The raw data was processed with MaxQuant v2.0.1.0 and searched with the Andromeda search engine against the murine SwissProt proteome database appended with common lab protein contaminants and the following modifications: Carbamidomethylation of C as a fixed modification and oxidation of M and protein N-terminal acetylation as variable ones. The LFQ (Label-Free Quantification) intensities were calculated and used for further calculations using Perseus v1.6.2.3. Decoy hits were filtered out. The LFQ intensities were log-transformed, and only proteins that had at least 3 valid values in at least one experimental group were kept. A normal distribution of the lower values of the data distribution was generated by Perseus software using a downshift of 1.8 and width of 0.3 in order to impute the remaining missing values.

CSF was collected from 4 NT, 4 untreated SOD1^{G37R}, and 4 MIF-treated SOD1^{G37R} mice. After examining the PCA it was clear that one of the samples from the untreated SOD1^{G37R} group was very different relative to all other samples and therefore was removed from downstream analysis.

RNA extraction and sequencing

RNA was extracted from the lumbar spinal cord using RNeasy plus mini kit (Qiagen), according to manufacture's protocol. The library was prepared using MARS seq in which the 3'UTR of the transcripts are captured and 8 bp Unique Molecular Identifiers (UMIs) are added to the DNA fragments to reduce errors and quantitative bias caused by the amplification. The samples were sequenced using illumina NovaSeq SP - 100 cycles.

Initial analysis of the raw sequence reads was carried out using the NeatSeq-Flow platform.[103] The sequences were quality trimmed and filtered using Trim Galore (v0.4.5) and cutadapt (v1.15). Alignment of the reads to the mouse genome (GRCm38) was done using STAR (v2.5.2a).[93] The number of reads per gene per sample was counted using RSEM (v1.2.28).[92] Quality assessment of the process was carried out using FASTQC (v0.11.8) and MultiQC (v1.0.dev0) Statistical testing for identification of differentially expressed genes, batch correction, gene annotation, clustering and enrichment analysis were performed with the DESeq2 module within the NeatSeq-Flow platform.[103] Batch correction was done using the SVA/Combat R package. Gene annotation was done using the "AnnotationHub" R package. The statistical analysis was done using the DESeq2[88] R package. For comparison (Contrast) between the different groups, the statistical model considered two effects: the treatment group and the batch. The analysis produced *p*p-value, FDR-adjusted *p*p-value and fold of change per gene. Genes with FDR adjusted *p*p-value <0.05 were considered Differentially Expressed (DE). Gene ontology (GO) was performed using ShinyGO.[27] Analysis was performed on 10 NT, 10 untreated SOD1^{G37R}, and 4 MIF-treated SOD1^{G37R} mice. The genes clustering was preformed using hierarchical clustering. Genes were considered as partially corrected if they were in a cluster where the expression in the MIF-treated group was between the NT group and not treated group, while genes were considered as highly corrected when the expression in the MIF-treated group was very close to the NT group.

qPCR of murine tissue

The murine RNA was transcribed to cDNA using the qPCRBIO cDNA synthesis kit (PCR Biosystems) according to manufacture's instructions. All PCR reactions were performed in triplicates, using fast SYBR green master mix (Applied Bioscience). Gene expression was normalized to GAPDH measured levels. Primers used are listed in Table S2.

RNA isolation and qPCR of human cell lines

The RNeasy kit (Qiagen, Hilden, Germany) was used for total RNA extraction of human cell lines according to the manufactures protocol. RNA was obtained from all differentiated cell lines and transcribed into cDNA using QuantiTect Reverse Transcription Kit (Qiagen, Hilden, Germany). Quantitative real-time PCR experiments were executed with cDNA from five ng of total RNA from at least three independent differentiations, 1.75 μM forward/reverse primer and Power SYBR-Green PCR Master Mix (Life Technologies, Carlsbad, USA). Relative levels of gene expression were normalized to healthy control. For further analysis the ddCt method was used and analysis settings according to the manufacturer's recommendation (threshold value 0.2) were applied using QuantStudio Real-Time PCR Software (Thermo Fisher, Walham, USA). Gene expression of MIF was normalized to PPIA+HPRT levels. Primers used are listed in Table S2.

Immunocytochemistry

Cells were fixed with cold 4% paraformaldehyde for 20 min at RT, washed carefully twice with PBS and incubated for 1 h in blocking solution (10% goat serum, 2.5% BSA, 0.6% Triton X-100) to block non-specific staining. Primary antibodies (mouse monoclonal anti-beta III tubulin (Tuj1) 1:1000; rabbit monoclonal Tuj1 1:1000; rabbit polyclonal anti-Map 2 1:1000; rabbit polyclonal anti-Islet1 1:1000; rabbit monoclonal anti-MIF 1:500 all from Abcam, Cambridge, UK and mouse monoclonal anti-Misfolded SOD1 (B8H10), Biomol

GmbH (Medimabs), Hamburg, Germany) were diluted in blocking solution and incubated overnight at 4°C. After two washing steps in PBS, fluorescently-labeled secondary antibodies Alexa Fluor 488 or 555 (goat anti-mouse IgG/IgG1/IgG2a or goat anti-rabbit IgG, 1:1000, Invitrogen, Carlsbad, USA) were diluted in blocking solution and added to the cells and incubated at room temperature for 2 h in the dark. Cells were then washed again twice with PBS and covered with Mowiol (Roth) according to the manufacturer's instructions. The secondary antibodies were tested for specificity and cross re-activity. Nuclear counterstaining with 4′,6-diamidino-2-phenylindole (DAPI, 10 μg/mL, Thermo Fisher Scientific) was performed in mounting solution. For each well at least two typical pictures were photographed at 20x magnification using an Olympus BX61 microscope equipped with an Olympus DP72 digital camera and the Olympus CellSens Dimension 1.18 program (Olympus, Hamburg, Germany) and finally analyzed with ImageJ.

Western Blots analysis

400-500 μL RIPA Buffer was added to each sample of human postmortem tissue with a subsequent homogenization step via sonication. The amount of total protein was measured with Pierce BCA Protein-Assay kit (Thermo Scientific, Walham, USA) according to manufactures protocol. An amount of 50 ng of total protein from each sample was mixed with Laemmli, denatured in a thermocylcer for 15 min at 95°C, then applied to an 8–16% Mini-PROTEAM TGX Precast Protein Gel (Bio-Rad Laboratories, Inc, Hercules, USA) and finally transferred to Nitrocellulose Blotting Membrane (Amersham Protan Premium, GE Healthcare Life Science, Chicago, USA) by standard procedures. Nonspecific binding sites were blocked with 5% nonfat dry milk (Sucofin, Zeven, Germany) in Tris-buffered saline (TBS), while antibodies were diluted in 5% BSA buffer (Sigma-Aldrich, Merck, Darmstadt, Germany). The following antibodies were used: MIF (rabbit 1:500, Abcam, Cambridge, UK) and α-Tubulin (mouse, 1:1000, Santa Cruz Biotechnologies, Dallas, USA). Primary antibodies were incubated overnight at 4°C. Detection was performed with suitable horseradish peroxidase-conjugated secondary antibodies (1:500; R&D System, Minneapolis, MN) followed by chemiluminescent substrate (SuperSignal West Pico PLUS; Thermo Scientific, Rockford, IL), and signals were detected by Chemolumineszenz Imager (Intas Science Instruments, Gottingen, Germany). The quantification was done by using LabImage1D software (Intas Science Imaging GmbH, Gottingen, Germany). Values were normalized to α-Tubulin.

Neuromuscular junction analysis

Plantaris and soleus muscles from both legs of the untreated and MIF-treated SOD1^{G37R} mice at postnatal day (P)355 (n = 4 mice per group) were dissected, and their fibers were teased under a dissecting microscope. These fibers were then pretreated with an antigen retriever solution (acidic citrate buffer, Millipore Sigma C999, 10 min at room temperature (RT), 15 min at +68°C in a humid chamber, 10 min at RT), washed and then blocked and permeabilized with a 1% BSA (VWR E588), 0.5% Triton X-100 (Sigma, USA) solution containing antibodies. To observe neuromuscular junction innervation and structure, the fibers were incubated overnight at RT with a primary solution containing a mouse-IgG1 anti- SV2 antibody (1:50, DSHB, USA) and a rabbit anti-β III Tubulin antibody (1:500, Abcam). After several washes, the fibers were incubated 1 h at RT with goat anti-mouse IgG1 Alexa 488 (1:500, Invitrogen, USA) and goat anti-rabbit Alexa 647 (1:500, Invitrogen, USA) secondary antibodies, plus an α-bungarotoxin (BTX) conjugated to rhodamine (1:500, Invitrogen, USA). The fibers were mounted onto slides with a glycerol mounting solution (50% glycerol, 50% 1X PBS, 0.03 mg/mL phenylenediamine), coverslipped, stored at −20°C and imaged on an inverted confocal microscope. Confocal image stacks were acquired with a 20 x 0.8 NA plan apochromat objective on a Zeiss LSM 880 confocal microscope (digital resolution: 1024 x 1024 pixels; zoom: 1; 16-bit depth; step size: 2 μm).

Answer ALS proteomics analysis

Whole-proteome extracts from frozen Answer ALS iPSC-derived MNs were digested and subjected to acquisition on the SCIEX 6600 as described previously.[36] Specifically, for MS analysis, digested peptides were resuspended in 0.1% FA and analyzed on a 6600 Triple TOF (Sciex) in data-independent acquisition (DIA) mode and on the 6600 Triple TOF (Sciex) for data dependent acquisition (DDA) mode.

Samples acquired in the DDA mode were used for sample specific library building. Raw intensity data for peptide fragments was extracted from DIA files using the open source openSWATH[104] workflow against the generated library. Target and decoy peptides were then extracted, scored, and analyzed using the mProphet algorithm[105] to determine scoring cut-offs consistent with 1% FDR. Peak group extraction data from each DIA file was combined using the 'feature alignment' script, which performs data alignment and modeling analysis across an experimental dataset and transition-level data is normalized by MS2TIC.

Batch correction was then performed on the transition-level using comBat[106] and LOESS[107] methods for correcting across and within samples of the digestion batches using the batch correction tool, BIRCH.[108] Correction was followed by missing value imputation using Random Forest (RF) method. The corrected and imputed data was then processed using the mapDIA[109] software to roll up fragment-level data to peptide and protein levels as well as to perform pairwise comparisons between ALS and control samples. Batch corrected proteomic expression data was further normalized using a variance-stabilizing transformation as implemented in the R package DEP. Pearson correlation was computed across all proteins in dataset (3495 unique proteins) for SOD1+ cases (n = 10) and all ALS cases (n = 175) (two outlier cases with MIF expression < Q1 - 2*IQR were previously removed). Statistical significance of association between proteins was assessed using the cor.test function in the R stats package, and FDR adjusted using the Benjamini-Hochberg method. Enrichment of upregulated MIF treatment-associated proteins among all MIF protein correlations was assessed using the minimum hypergeometric test, as implemented in the R package mHG.

QUANTIFICATION AND STATISTICAL ANALYSIS

Statistical analysis

Statistical analysis was preformed using Originlab Pro. Analysis started by performing normality test for all groups, in case of normal distribution, t-test was used to compare two groups and one-way ANOVA followed by Tukey's multiple comparison test was used when more than two groups were compared. In cases where normal distribution was rejected, Mann-Whitney U test used to compare two groups and Kruskal-Wallis one-way ANOVA followed by Dunn's multiple comparison test was used to compare more than 2 groups. Graphs represent the mean and whiskers represents standard error (SE). All data of healthy control and ALS cell lines were pooled in control and mutant genotype (SOD1, C9orf72, TDP43 and FUS) groups and are presented as mean ± SEM. Results were regarded as statistically significant with $p < 0.05$.